



Control of structural damage on the rock mass characteristics and its influence on the rock slope stability along National Highway-07, Garhwal Himalaya, India: an ensemble of discrete fracture network (DFN) and distinct element method (DEM)

Jaspreet Singh¹ · Sarada Prasad Pradhan¹ · Mahendra Singh² · Lal Hruaikima²

Received: 18 January 2021 / Accepted: 13 January 2022 / Published online: 12 February 2022
© Springer-Verlag GmbH Germany, part of Springer Nature 2022

Abstract

The existing structural discontinuities such as faults, joints and cleavages in rock slopes control the rock mass properties. The presence of structural discontinuities is strongly influenced by the regional tectonic structures. The concept of damage as applied to intact rock and rock mass relates to the degradation of their strength properties. The high variability in fracture intensity and trace length has been found as one move away from the hinge zone due to damage caused by regional syncline in Garhwal Himalaya. The high in situ stresses in fold hinge zone during folding propagated the fractures utmost and result in a high frequency of mean-sized fractures. The high fracture intensity and nearly equal joint traces intersected comparatively smaller-sized blocks. Whereas the rock mass away from the damage zone (fold core) at sites 2 and 3 comprises low fracture intensity and intersects relatively larger-sized blocks. Deterministic and stochastic DFN approaches were implemented in 3DEC to model the rock mass conditions within and away from damage zone. The study provided a comprehensive insight into rock mass behavior using structural investigation and numerical modeling. The work concluded that the high fracture intensity in fold hinge zone reduced the rock mass strength, providing the kinematic freedom to blocks resulting in slope failure.

Keywords Discrete element method (DEM) · Discrete fracture network (DFN) · Joints · Syncline · Damage zone · Slope stability

Introduction

Slope failures are governed by many factors, such as geological, geomorphological, hydrological, and geotechnical. Engineering projects require the excavation of the soil or rock and the stability of these cut slopes is a prime concern for safety. The structural features such as folds, faults, joints, and shear zones contribute to the instability in the rock mass depending upon their orientation to the slope and rock mass damage associated with them (Stead and Wolter 2015; Singh and Thakur 2019). When the shear stresses acting along potential failure surfaces

overcome the shear strength, the material fails. Several authors have reported the high variation in fracture distribution in structurally damaged zones (Savage and Brodsky 2011; Johri 2012; Pedrazzini et al. 2011; Pradhan et al. 2018). Damage zones are regions of anomalously high fracture density surrounding larger-scale geological structures (Johri 2012). Savage and Brodsky (2011) suggested that the fracture density (F , i.e., the number of fractures/meter) decays with distance from isolated faults following a power law. Shipton and Cowie (2003) reported various types of damage associated with the geological structures. Brideau et al. (2009) and Pradhan et al. (2020) have investigated several landslides and found the importance of rock mass damage on slope instability. The rock mass failed at Aishihik River Landslide, Hope Slide, and East Gate Landslide due to folding and faulting associated with tectonic deformation (Brideau et al. 2009). A considerable reduction was found in Geological Strength Index (GSI) near the tectonic structures (Budetta and Nappi 2011; Brideau et al.

✉ Sarada Prasad Pradhan
sppradhan@es.iitr.ac.in

¹ Department of Earth Sciences, Indian Institute of Technology Roorkee, Roorkee, India 247667

² Department of Civil Engineering, Indian Institute of Technology Roorkee, Roorkee, India 247667

2009). Stead and Wolter (2015) have also discussed the probable failure modes associated with different types of folds. Pedrazzini et al. (2011) demonstrated the rock mass damage related to folding and its influence on slope stability at Turtle Mountain, Canada.

3D block stability analysis techniques provide more realistic outputs and allow complex movement of the block in all dimensions along bounding surfaces. Digital photogrammetry (DP) and laser scanning (LS) are effective surveying techniques that help to produce 3D topography and conducting discontinuity survey of the slope with high precision. Previous slope stability investigations in rocky slopes have empathized the influence of discontinuities on the slope instability (Brideau et al. 2012; Coggan and Pine 1996; Havaej et al. 2015; Donati et al. 2017; Singh et al. 2013, 2019; Vishal et al. 2015). Havaej et al. (2015) have used the combined remote sensing and discrete fracture network (DFN) techniques for simulating kinematic block failure in the UK-based mine quarry slope and found a considerable effect of discontinuities on block stability. DFN is considered a reliable technique to incorporate the uncertainty in synthetic rock mass modeling and characterization. Elmo and Stead (2010) successfully integrated numerical modeling–discrete fracture network (DFN) approach for characterization of the strength of naturally fractured pillars. Recently, Vanneschi et al. (2019) employed a distinct element method using a complex volumetric mesh model to simulate direct toppling and identified unstable blocks in the area of high slope angles and validated with the field conditions. Brideau et al. (2011) used the DEM method for stability analysis of South Peak, Crowsnest Pass, Alberta, Canada, to determine the influence of individual discontinuity sets, friction angle and scale effects. Many authors have investigated the impact of rock bridges and discontinuities using FEM, DEM, and hybrid numerical modeling codes (Bonilla-Sierra et al. 2015; Costa et al. 1999; Havaej 2015; Elmo et al. 2011; Sturzenegger and Stead 2012; Brideau and Stead 2012; Elmo and Stead 2018; Pradhan et al. 2018; Pradhan et al. 2019; Viviana et al. 2015). Shaunik and Singh (2019, 2020) conducted experimental studies to examine the impact of non-persistent discontinuity on the strength of the rock mass.

The damage associated with geological structures has considerable influence on the rock mass and the associated structural geological characteristics are strongly dependent upon couple of factors such as local geology, tectonic settings, in situ stresses, petrological and mechanical properties of the rocks. The objective of this paper is to investigate the damage caused by the geological structure (Garhwal Syncline) to the rock mass and its practical implication to the slope failures. We do not provide a conclusive argument that the damage induced by every geological structure would be the same everywhere but instead could show similar fracture characteristics. The

study compares the rock mass characteristics within and away from the damage zone and their influence on slope stability. The rock mass from all the sites was modeled by DEM based numerical modeling using deterministic and stochastic approaches. In the stochastic approach, the generated DFNs were imported into 3DEC for slope stability analysis. The focus was to highlight the importance of regional-scale geological structures in engineering geological practices and their influence on rock mass characteristics.

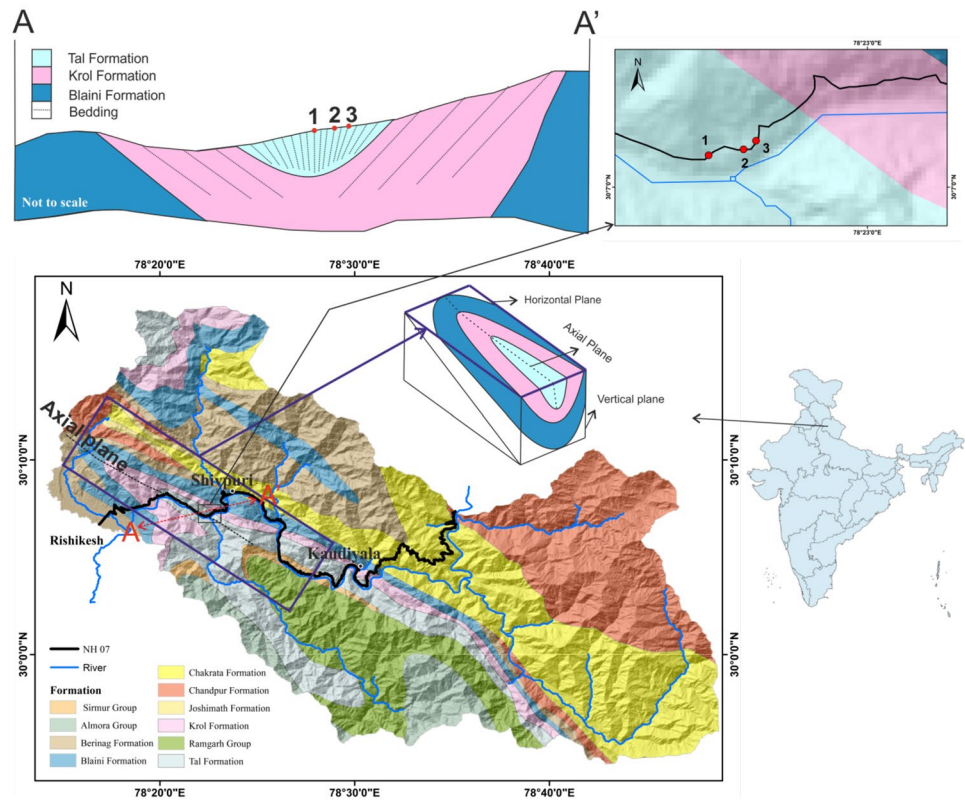
Geological and structural settings

The study area lies along the NH-07 road section in the Garhwal Lesser Himalaya (Fig. 1). The Krol group of rocks comprises Blaini, Krol and Tal Formations (Valdiya 1984). A continuous sequence of different members of the Krol and the Tal Formation are exposed along the road section from Rishikesh to Shivpuri. Further from Shivpuri towards Kaudiyala, the Blaini Formation is exposed along the road section overlaid by Krol and Tal Formations. The Krol Group is part of a regional-scale syncline known as Garhwal Syncline. The Tal Formation is divided into Upper and Lower Tal Formations (Shankar 1971; Shanker et al. 1993). The Lower Tal comprise of chert, arenaceous, argillaceous and calcareous members. The Lower Tal Formation is well developed in the Garhwal Syncline, particularly in the northern limb of the syncline between the Kaudiyala and Singtali localities in the Alaknanda valley. Upper Tal Formation dominantly consists of ortho-quartzite and arkosic sandstone and partial partings of mudstone. Tal Quartzite is a mature, medium- to coarse-grained ortho-quartzite with large-scale cross laminations and unfossiliferous (Shanker et al. 1993). Cambrian Tal Formation is unconformably followed by Cretaceous anikot Shelly Limestone and unconformably overlain by the Eocene Subathu Formation. The sandstone (Ortho-quartzite) of Tal Formation was found in the hinge zone (core) of regional Garhwal Syncline. The folding of beds is perceptible in the geological map that can be inferred from the repetition of beds along the line “AA” in Fig. 1, and the dashed line marks the hinge zone. The conceptual diagram of syncline can be found in Fig. 1 and shows the SE plunging fold. The stratigraphic section of Garhwal Syncline is listed in Table 1.

Methodology

Three different approaches were combined for 3D modeling of the slope, i.e., digital photogrammetry survey, discrete fracture network and distinct element modeling.

Fig. 1 Geological map of the study area (After Valdiya 1984)



Digital photogrammetry using a simple handheld camera was used to develop a 3D point cloud of the slope. The 3D point cloud was used to extract useful geological data and slope topography construction. The developed 3D

topography was imported into distinct element code for slope stability investigations. The methodology opted for the study is discussed below in detail.

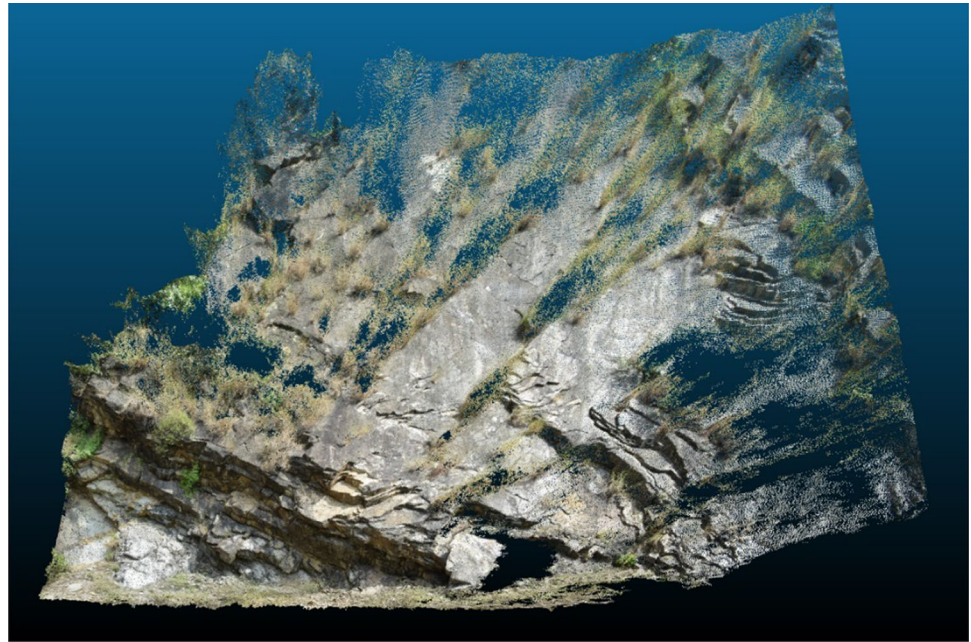
Digital photogrammetry survey

Photogrammetry is the science and technology of obtaining reliable information about physical objects through capturing, measuring and interpreting images. A terrestrial handheld camera was used for photo acquisition of the slope from different line of sights for overlapping. The digital camera used for digital photogrammetry (DP) surveying was a Nikon D5300 and the technical specifications are as follows: sensor size 23.5 mm × 15.6 mm, 24.2 million effective pixels, and maximum image dimensions of 6000 × 4000 pixels. During photo acquisition in the field, the lens with a focal length of 18 mm was used. It is possible to calculate the area acquired by a photograph by using the distance between the target and the camera using Eq. 1 (Francioni et al. 2018, 2019), where f is the focal length of lens, L is the distance between lens and object, AB is the width of slope and CD is the width of camera lens. Considering the width of the image 23.5 mm and 18 mm focal length, the area acquired by photograph will be of width 9.14 m when the distance between the camera and target is 7 m. The distance calculated between two consecutive locations is 1.82 m for an

Table 1 Stratigraphical setup of Garhwal Syncline (Shanker et al. 1993)

Formation	Rock type	Age	
Subathu	Grey–green shale	Paleocene–Eocene	
	Unconformity		
Manikot limestone	Limestone	Cretaceous	
	Unconformity		
Tal	Upper Tal	Arenaceous Cambrian	
	Lower Tal	Calcareous	Early Cambrian
		Arenaceous	
		Shale	
	Chert		
Krol	Dolomite	Pre-Cambrian	
	Shale		
Blaini	Diamictite	Pre-Cambrian	
	Quartzite		
	Phyllites		

Fig. 2 Developed point cloud using photogrammetry of a slope along NH-07 for topography construction



80% overlapping of the images adopting the fan method for photo acquisition. Structure from Motion (SfM) is a technique in which multiple overlapping 2D photos are used to construct the 3-dimensional structure of an object. Agisoft Photoscan software uses the concept of SfM for generation of 3D point cloud using multiple overlapping 2D images. A user must load a series of overlapping photos procured as discussed above, the software automatically detects discernible features within each photo and connect the features to construct a 3D model. For perfect matching, the user must manually match the features in the photographs. The developed point cloud was georeferenced before using it in final analysis. Total station was used to provide the coordinate of points on the slope to scale the point cloud. The developed point cloud was later used for 3D topography construction and discontinuity-related data extraction using Cloud compare (GPL Software 2018) (Fig. 2).

$$\frac{f}{L} = \frac{CD}{AB} \quad (1)$$

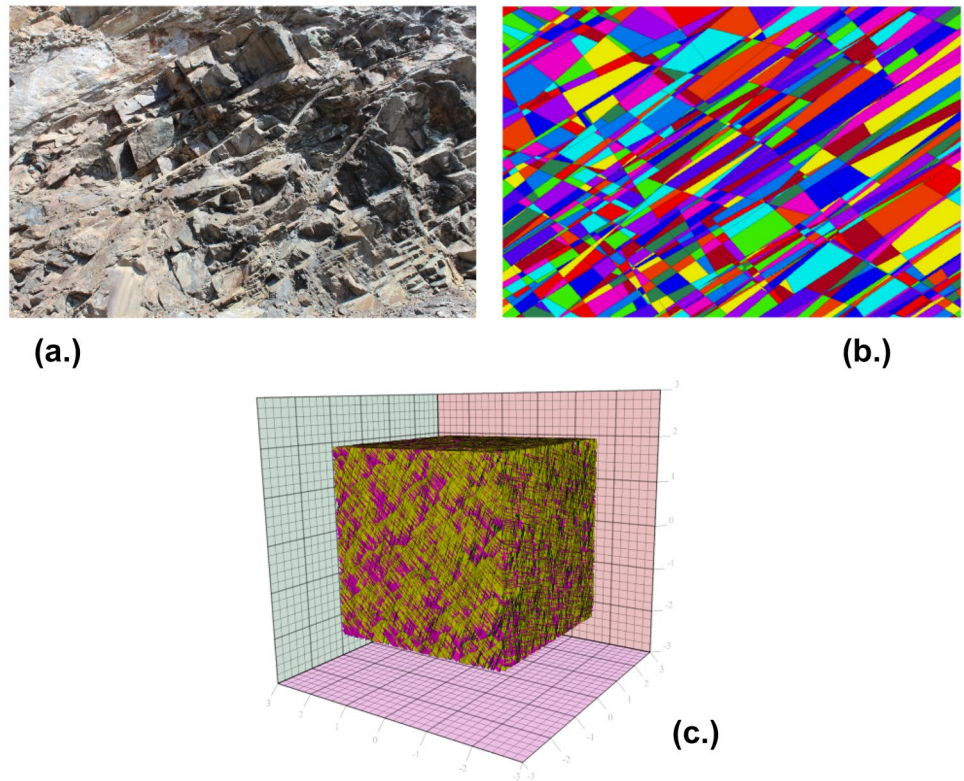
Discrete fracture network (DFN)

The DFN approach is a modeling methodology that uses statistical methods by creating a series of fractures that describe the rock mass fracture system (Elmo 2006; Dershowitz et al. 2014). The stochastic approach builds fractures at random locations following the given parameters. The input parameters for DFN modeling include fracture orientation distribution, fracture density or length distribution for assigning maximum and minimum threshold of area or trace length. Different type of fracture densities/intensities were discussed by Dershowitz and Herda (1992) and developed P_{ij} system for fracture intensity measurement used in DFN development. The most widely used fracture intensities are P_{21} and P_{32} defined as the cumulative length of fractures per unit area and the cumulative area of fractures per unit volume, respectively. Elmo (2006) and Pine et al. (2006) had extensively discussed the generation process of DFN for application in geomechanical

Table 2 Mechanical properties of intact rock, rock mass and joints used in the simulation

	Intact rock modulus (GPa)	Rock mass modulus (GPa)	Joint normal stiffness (GPa/m)	Joint shear stiffness (GPa/m)	Joint friction	Unit weight (kN/m ³)	UCS (MPa)	GSI
Site 1	4.83	0.216	0.75	0.075	35°	27	59.2	35
Site 2	4.83	0.71	1.38	0.138	35°	27	61	55
Site 3	4.83	0.71	1.38	0.138	35°	27	58.6	55

Fig. 3 **a** Rock slope in the field (site 2); **b** DFN imported into 3DEC; **c** Generated DFN for site 2 having three joint sets colored yellow, pink, and dark green (not to scale).



analysis. Discrete fracture networks (DFNs) have wide applicability in civil, mining, and geological engineering. The DFN are commonly used to estimate the fragmentation distributions, kinematic block stability and groundwater flow into mines. In context to synthetic rock mass (SRM) models, the DFNs are primarily used

for rock mass deformation and strength estimation. The work includes the application of DFN for kinematic block stability at three different slopes, using DEM to examine the influence of structural damage on the rock block stability. The in situ block volume distribution was also plotted for blocks size analysis formed by intersection of

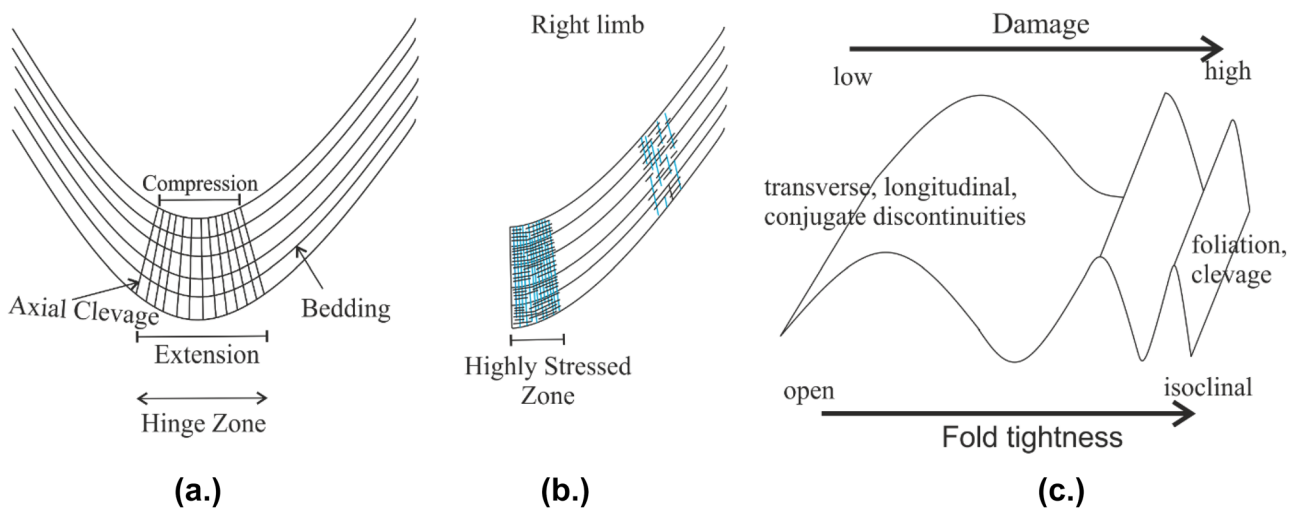


Fig. 4 **a** Conceptual model of the syncline; **b** fractures associated with folding in the right limb of the syncline with high fracturing in the hinge zone (core) because of profound stress accumulation during

folding mechanism; **c** damaged induced to rock mass with increase in fold tightness (Modified after Brideau 2005; Stead and Wolter 2015).

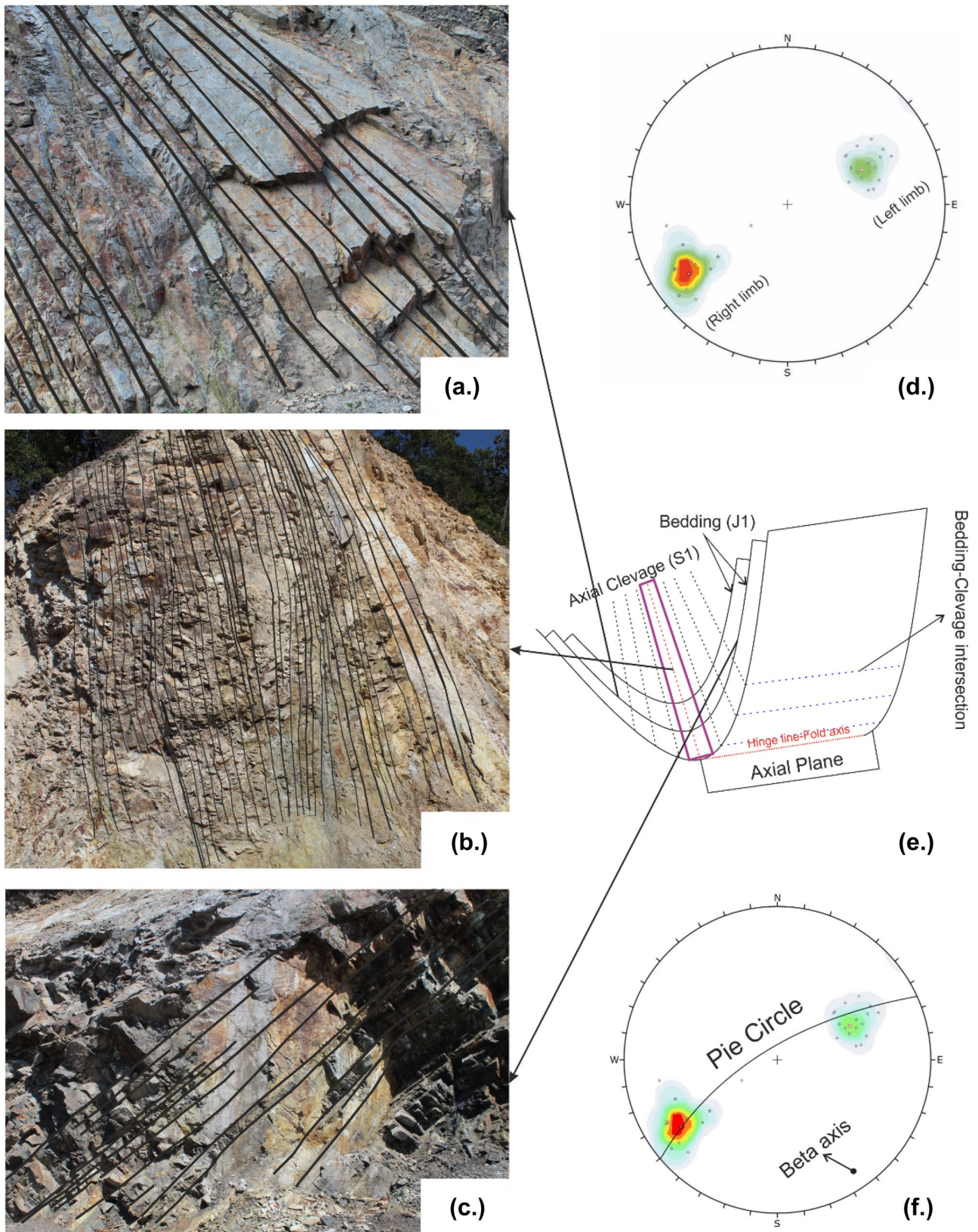


Fig. 5 180-degree change in the dip direction of the joints parallel to bedding in Sandstone (Tal Formation) along the road section from **a–c** marking the presence of syncline (Core of regional-scale Garhwal

Syncline); **d** poles to bedding plane plotted over stereonet showing the presence of fold limbs; **e** conceptual model of the syncline; **f** pie diagram showing pie circle and the beta axis (fold axis)

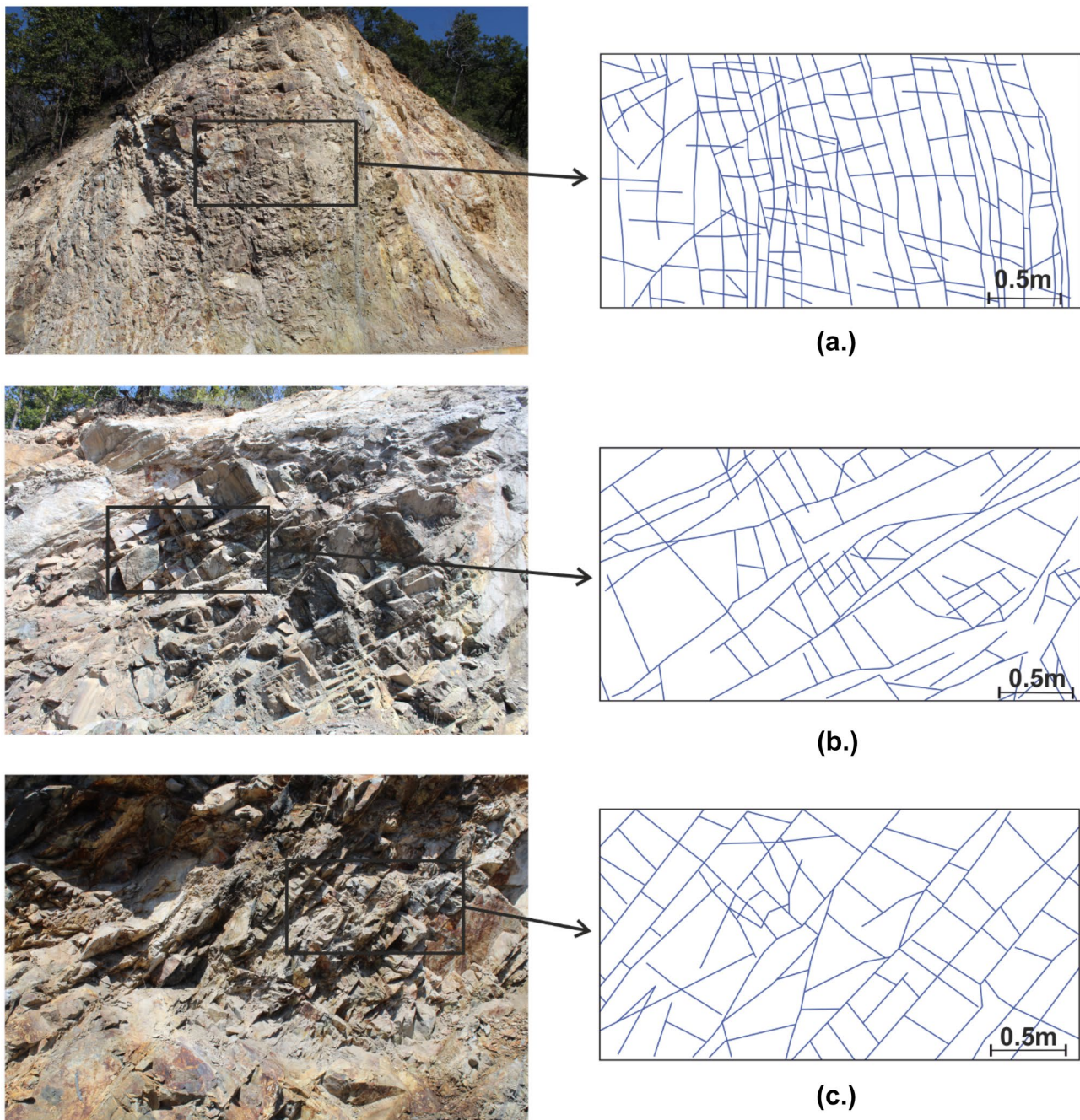


Fig. 6 Shows the rock mass and traced blocks formed by the intersection of discontinuities at three different sites: **a** site 1; **b** site 2; **c** site 3

discontinuities at each site using DFN. Based upon the field traced data the 3D fracture network was generated using DFN for all the three sites in PFC 5.0 and later imported into 3DEC geometry model for slope stability analysis. Figure 3a shows the field photograph of the rock mass at site 2. Figure 3b shows the screenshot of 3DEC model with multiple blocks formed by the intersection of DFN.

Distinct element modeling (DEM)

The discrete element method (DEM) is a numerical technique used to simulate independent particles' behavior. Multiple discontinuities in a rock mass result in the formation of blocks that can independently interact. The complexities related to discontinuity sets and different failure

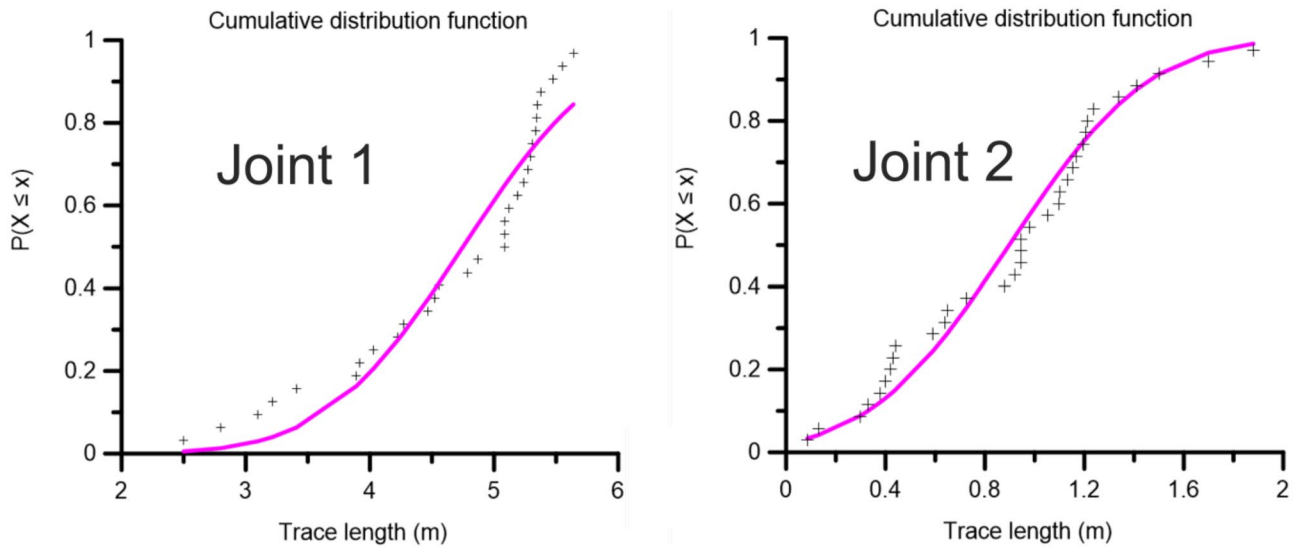


Fig. 7 Cumulative distribution function of trace lengths for the fracture sets in fold damage zone (hinge zone) at site 1 showing log-normal fit. (The solid line shows the log-normal fit assigned to the data and the plus sign represents each fracture data)

modes can be modeled using the distinct element method. To understand the block failures associated with discontinuity parameters in the rock mass, a 3D distinct element code, 3DEC 5.2 was used (Itasca Consulting Group Inc 2017a). eSignificant rotation and movement of blocks are allowed along the bounding discontinuities in distinct element modeling. Moreover, the blocks can be considered both rigid and deformable, depending upon the requirement. The objective of the study was to examine the influence of discontinuities due to structural damage on the kinematic block stability in three different rock mass conditions. The height of the slope is low, the maximum vertical stress at the base of slope with a height of 15 m will be approximately 4 MPa, which is very low compared to the UCS of intact rock. So, the blocks were considered rigid to understand the discontinuity-controlled nature of the rock mass. The USC test of the intact rock was conducted in laboratory on a NX core and found to be around 60 MPa. The unit weight of the rock was also estimated in laboratory from NX core and found to be 27 kN/m³ and intact rock modulus of the sample was 4.83 GPa. Moving to joint parameters, there are different failure criteria like Mohr–Coulomb, Barton-Bandis and Patton’s model that addresses the shear strength behavior of the rock joint or discontinuity. Among them, Mohr coulomb is the most simple and commonly adopted failure criteria which states that there is a linear relationship between shear and normal stress at failure. It is easy to estimate the parameters cohesion and friction of the rock joint. No filling was noticed in the joints and the surface was found to be smooth. Depending upon the observation the joints were considered cohesionless and

the friction angle was estimated using portable tilt test in the field and found to be 35°. The normal stiffness parameters of joints were estimated using the empirical relation given in Eq. 2 (Barton and Choubey 1977), where E_i , E_m , and l are Intact rock modulus, Rock mass modulus and joint spacing respectively. The rock mass modulus was calculated empirically using Roc Lab software (Rocscience 2014). The shear stiffness is generally considered as one-tenth of the normal stiffness (Barton and Bandis 1990). The mechanical parameters used in empirical relations and directly in simulation are listed in Table 2. Generally, in 3D modeling, the slope geometry is oversimplified by just considering a plane with a given orientation. To model the complexities in slope topography, point cloud was used to generate mesh for the construction of slope geometry. Slope topography was shaped in 3DEC using the “octree” approach to heed the blocky nature of the slope (Itasca Consulting Group Inc 2017b).

$$K_n = \frac{E_i * E_m}{l * (E_i - E_m)} \tag{2}$$

Table 3 Joint persistence calculated using joint spacing (J) and mean joint spacing (J_m) for the 3DEC model

	Length of a scanline (L)	No. of joints (N)	Mean spacing (L/N)m	Persistence (joint spacing (J)/mean spacing (J_m))
1	7 m	28	0.25	0.25/0.25 = 1.0
2	7 m	21	0.33	0.25/0.33 = 0.75

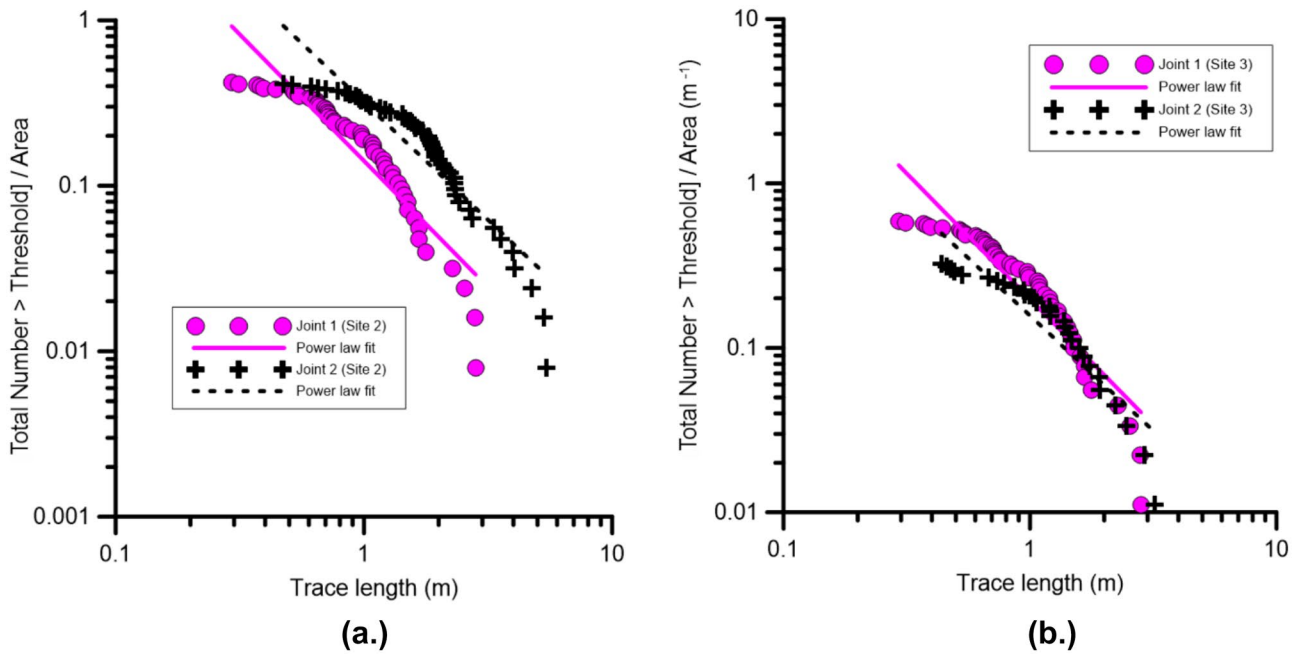


Fig. 8 Cumulative length distribution of trace lengths for the fracture sets at sites away from hinge zone showing power-law fit. (The solid and dashed lines shows the power-law fit assigned to the data and the plus and dot sign represents each fracture data) **a** site 2; **b** site 3

Geological field investigations

To probe the implications of regional Garhwal Syncline on the rock mass characteristics, three different sites were selected. Site 1 lies within the hinge zone, whereas sites 2 and 3 lie on the right limb of the syncline away from the hinge zone (Figs. 1 and 6). Damage zones represent a network of subsidiary structures surrounding the fault/fold core, which are mechanically related to the fault zone/fold because of high in-situ tectonic stresses (Chester and Logan 1986; Smith et al. 1990). The relatively undeformed rock material free from fault/fold-related structures also surrounds the damage zones. The concept of damage as applied to intact rock and rock mas relates to the degradation of their strength properties (Brideau 2005).

Folds are the geological structures that develop when a planar geological stratum bends into a wavy form having crest and trough due to ductile deformation under high compressive stresses (Fig. 4). The anticline is formed when beds dip away from each other and Syncline (Figs. 4 and 5) is formed when the beds are dipping towards each other. The folding of beds is perceptible in the geological map also, which can be inferred from the repetition of beds along the line “AA” in Fig. 1, and the hinge zone is marked by the dashed line (Fig. 1). Based upon the field structural data plotted over stereonet, the concentration of the poles to bedding planes can be found demarcating the limbs of the Garhwal Syncline (Fig. 5d). The pie diagram shows the trend of the fold axis of the syncline which matches as observed on the geological map (Fig. 5f). The fold hinge is

Table 4 Calculation of persistence value for bedding joint (J1) from the mean joint spacing (J_m) and joint spacing (J) for the rock mass at three different sites

Site	Length of a scanline (L)	No. of joints (N)	Mean spacing (L/N)	Persistence (joint spacing (J)/mean spacing (J_m))
1	8.52 m	28	$(0.30 + 0.318)/2 = 0.30$ m	$0.3/0.3 = 1$
	8.27 m	26		
2	7.68 m	13	$(0.59 + 0.59 + 0.676)/3 = 0.61$ m	$0.3/0.6 = 0.5$
	9.59 m	16		
	5.41 m	8		
3	4.56 m	3	$(1.52 + 0.68 + 0.55)/3 = 0.91$ m	$0.34/0.91 = 0.37$
	6.80 m	10		
	7.74 m	14		

the line joining points of maximum curvature on a folded surface and it is the zone where maximum strain accumulation takes place. Figures 4 and 5e depict the conceptual model of the syncline and fracturing associated with it (Brideau 2005; Price and Cosgrove 1990).

During geological investigations, pronounced variation was observed in the joint spacing and intensity of the joints as one moves away from the hinge zone (damage zone) of the regional Syncline (Fig. 6). Discontinuity trace lengths have dominant control over rock mass behavior and rock slope stability. Several authors have investigated discontinuity trace length and found that it typically follows log-normal, negative exponential or power-law distributions (Srivastava 2002; Vazaios et al. 2018; Elmo 2006). In this study, log-normal trace length distribution was a good fit with discontinuity trace length data at site 1 (Fig. 7). Further, at sites 2 and 3, the power-law distribution provides a suitable fit (Fig. 8). Among the three joint sets, two joint sets were impeccably traceable at all three sites, while traces for the third were obscure due to excavation. The data for the third joint was collected with few assumptions and judgments in the field.

The axial cleavage or bedding joints were having uniform spacing and approximately equal trace lengths (following a log-normal distribution) at site 1 in the damage zone associated with fold hinge (Figs. 6a and 7). Fracture propagation occurs within the natural material because of the applied stresses; still, their distribution may be halted by the eradication of applied stresses or the existence of a weak interface like joints that arrests the propagating crack (Vazaios et al. 2017; Mandl 2005). The high in-situ stresses in the damage zone around the fold hinge provided the pathway for fracture propagation, overcoming all the barriers, and resulted in high fracture intensity (Brideau 2005). Fracture propagation leads to fractures with a high frequency of comparatively equal trace lengths following log-normal distribution and combined with high fracture intensity (Table 5) intersected blocks of small size or volume (Figs. 6a and 9). Due to intense folding in the hinge, the bedding joint becomes almost vertical and parallel to the axial cleavage. The axial cleavage (S_1) develops perpendicular to the principal axis of shortening during folding (Figs. 4a and 5e) (Fossen 2010). The stresses associated with folding create new fractures parallel to axial cleavage or propagate existing ones, i.e., bedding joints (S_0), and lead to the high consistency of the fracture trace lengths in the hinge zone. Stead and Wolter (2015) have also discussed the increase in damage with folding with the highest damage associated with highly folded or isoclinal folds (Fig. 4c). Further, at sites 2 and 3, as one moves away from the hinge zone along the right limb of a syncline, the mean joint spacing is comparatively high due to low fracture intensity (Table 5) (Fig. 6b, c). Also, the fracture trace lengths at sites 2 and 3 follow power-law

Table 5 Parameters for DFN generation for the three different sites

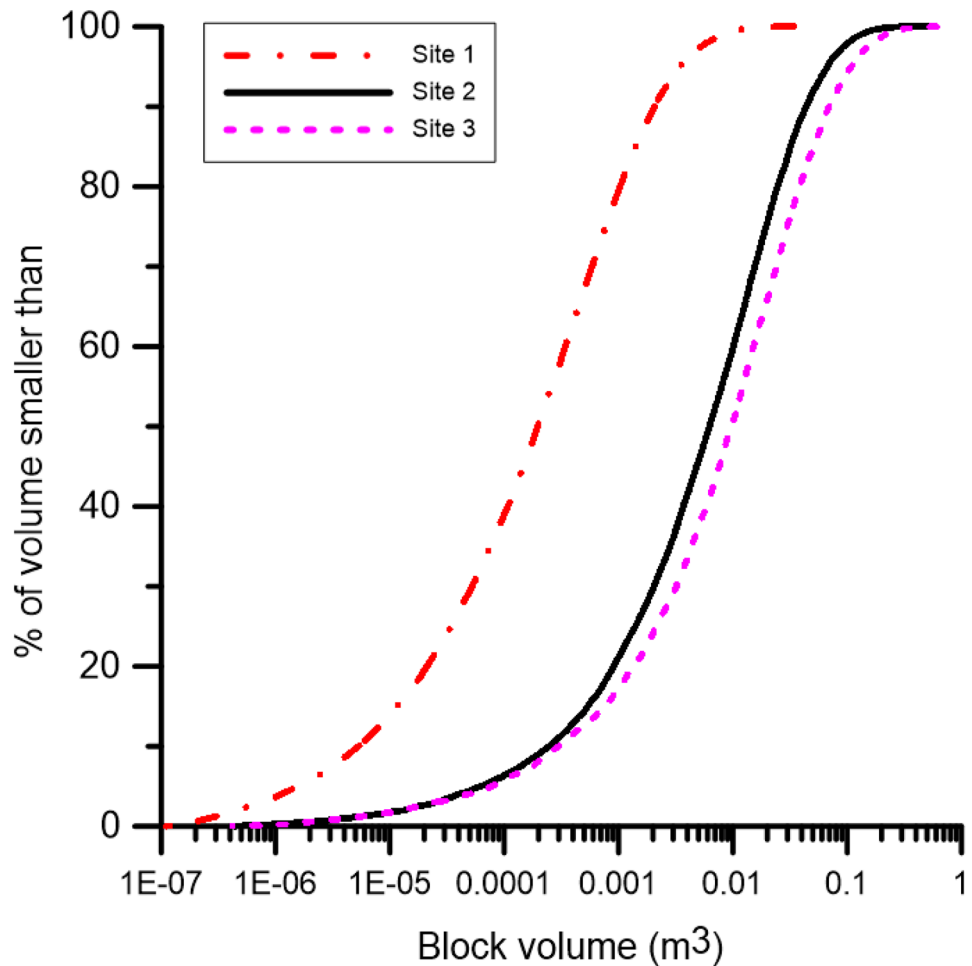
Sites	Joints	Properties	Distributions	Parameters
1	J1	Length (m)	Log-normal	Mean \pm Std: 4.75m \pm 0.87
		Orientation	Fisher	Dip/Dip direction: 80/80
		P_{32} (m^{-1})		4.5
	J2	Length (m)	Log-normal	Mean \pm Std: 0.9m \pm 1.23
		Orientation	Fisher	Dip/Dip direction: 45/165
		P_{32} (m^{-1})		3.9
	J3	Length (m)	Log-normal	Mean \pm Std: 1.3m \pm 1.7
		Orientation	Fisher	Dip/Dip direction: 75/320
		P_{32} (m^{-1})		4.2
2	J1	Length (m)	Power-law	Alpha: 2.229
		Orientation	Fisher	Dip/Dip direction: 45/240
		P_{32} (m^{-1})		0.7995
	J2	Length (m)	Power-law	Alpha: 2.528
		Orientation	Fisher	Dip/Dip direction: 60/150
		P_{32} (m^{-1})		0.66
	J3	Length (m)	Power law	Alpha: 2.4
		Orientation	Fisher	Dip/Dip direction: 35/30
		P_{32} (m^{-1})		0.62
3	J1	Length (m)	Power law	Alpha: 2.528
		Orientation	Fisher	Dip/Dip direction: 45/240
		P_{32} (m^{-1})		0.863
	J2	Length (m)	Power-law	Alpha: 2.519
		Orientation	Fisher	Dip/Dip direction: 60/150
		P_{32} (m^{-1})		0.451
	J3	Length (m)	Power-law	Alpha: 2.6
		Orientation	Fisher	Dip/Dip direction: 35/30
		P_{32} (m^{-1})		0.55

distribution, i.e., high frequency of comparatively small-sized fractures (Fig. 8). The smaller trace length of the joints is a result of declined in-situ stresses along the limb during folding that halted the fracture propagation (Chester and Logan 1986; Brideau 2005). Low fracture intensity and smaller fracture trace length intersect block of comparatively larger size or volume (Figs. 6b, c and 9). The blocks intersected at sites 2 and 3 are almost equal-sized and greater than site 1. The block volume at each site 1, 2 and 3 was found using DFNs, which will be discussed in a later section.

Numerical modeling setup

To examine the control of structural damage over block kinematics, field conditions of different sites were modeled in 3DEC for three-dimensional simulations of block stability. A fixed 3d topography was used to simulate rock mass of different sites with divergent conditions to eradicate the control of slope topography and orientation.

Fig. 9 Block volume distribution curves of blocks intersected using generated DFNs for sites 1, 2 and 3

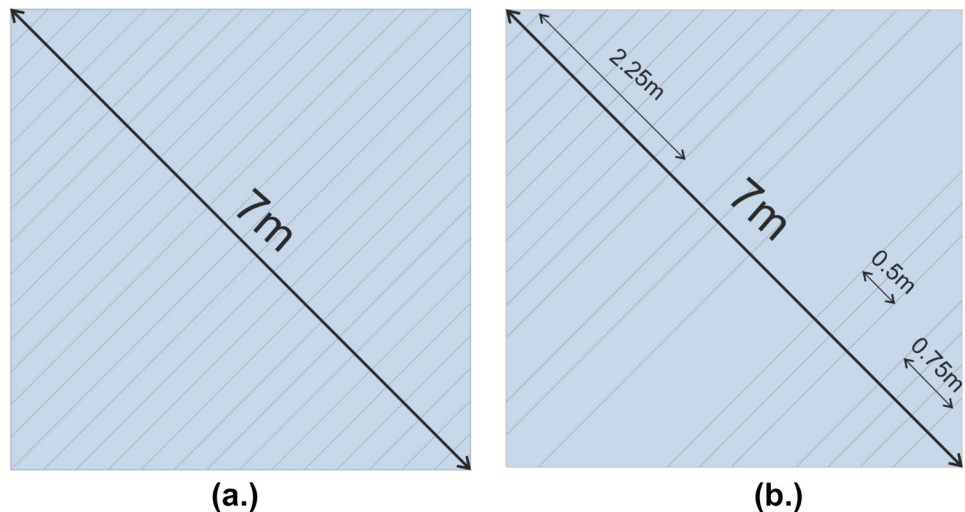


Deterministic approach

To model the slope rock mass, first, the deterministic approach with fixed joint orientation was used. The variability in joint spacing was modeled using the persistence parameter in 3DEC. It is too complex to use the

stochastic method everywhere because of large data availability for developing probability distribution curves and requires high computation time. As joint termination leads to an increase in the spacing of other joint sets, alternately, the joint persistence parameter in 3DEC was implemented to simulate the rock mass with varying joint spacing.

Fig. 10 **a** 3DEC model with joint persistence 1.0; **b** 3DEC model with joint persistence 0.75, the decrease in joint persistence lead to increase in the mean joint spacing (J_m) compared to figure (a). Note: Joint spacing (J) is considered 0.25 m in both the models



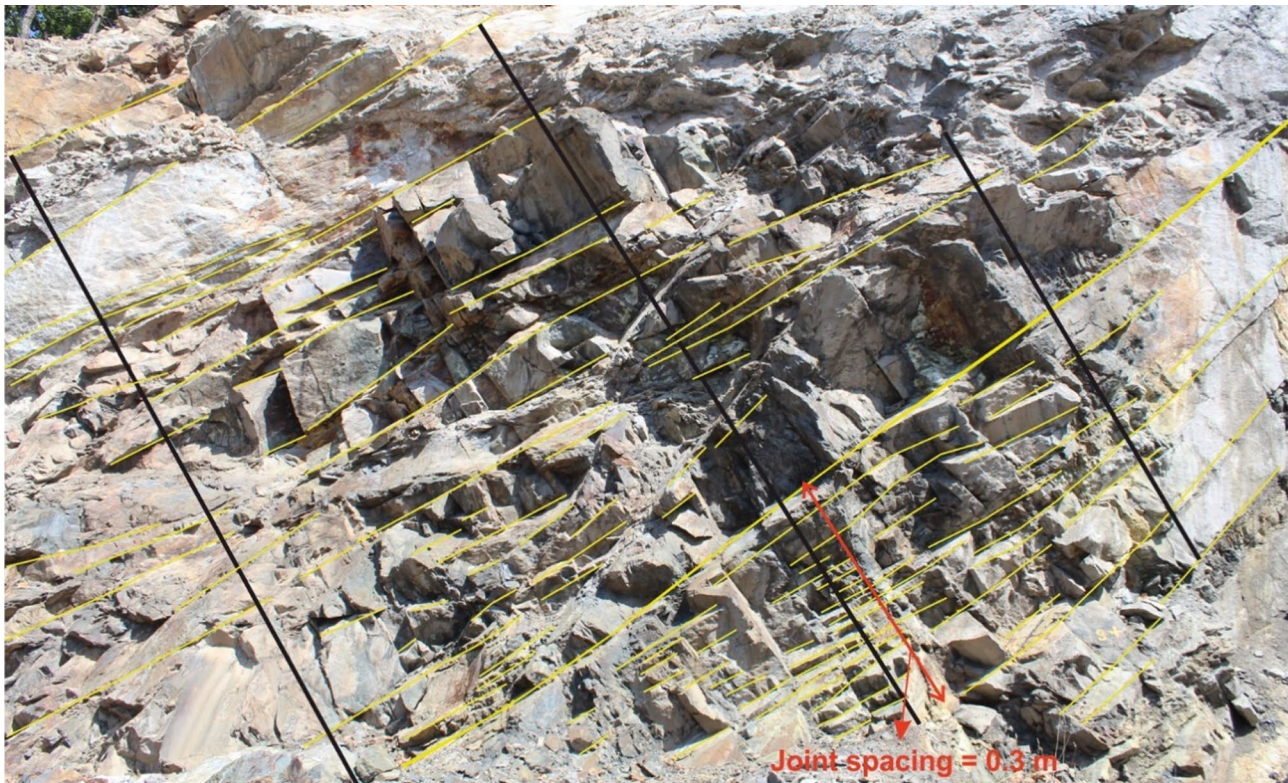


Fig. 11 Scanlines marked over the rock mass to calculate the joint persistence parameter of the bedding joint set (J1) at site 2 used in 3DEC model construction

The persistence parameter develops a stochastic models of the joint network having equal mean joint spacing. Persistence (p) is the probability that any given block lying in the path of a joint will split (i.e., if $p=0.5$, then 50% of the block will break) (Itasca Consulting Group Inc 2017b). Two 3DEC block models are shown in Fig. 10 constructed with different joint persistence values 1.0 and 0.75, respectively; joint spacing (J) was considered the same as 0.25 m in both the models. The mean joint spacing (J_m) for the resultant modeled rock mass is different for both the models with 0.25 m and 0.33 m respectively. The length of the scanline should be at least five times greater than the joint spacing for acceptable results (Priest and Hudson 1976). The cluster of joints with smaller spacing can be found in the rock mass (Figs. 10b and 11) and used to calculate joint spacing (J) whereas the mean joint spacing (J_m) is calculated for whole joint set. The formula associated with the calculation of joint persistence from joint spacing (J) and mean joint spacing (J_m) for the 3DEC model is shown in Table 3. To find the mean spacing of bedding joint (J1) average of mean joint spacing (J_m) from all the scanlines was taken (Fig. 11). Table 4 shows the joint spacing and joint persistence parameter calculated for the bedding joint (J1) at all the three sites. Similarly, the persistence and the joint spacing parameters were calculated for the other two joint sets used in numerical modeling.

Stochastic approach

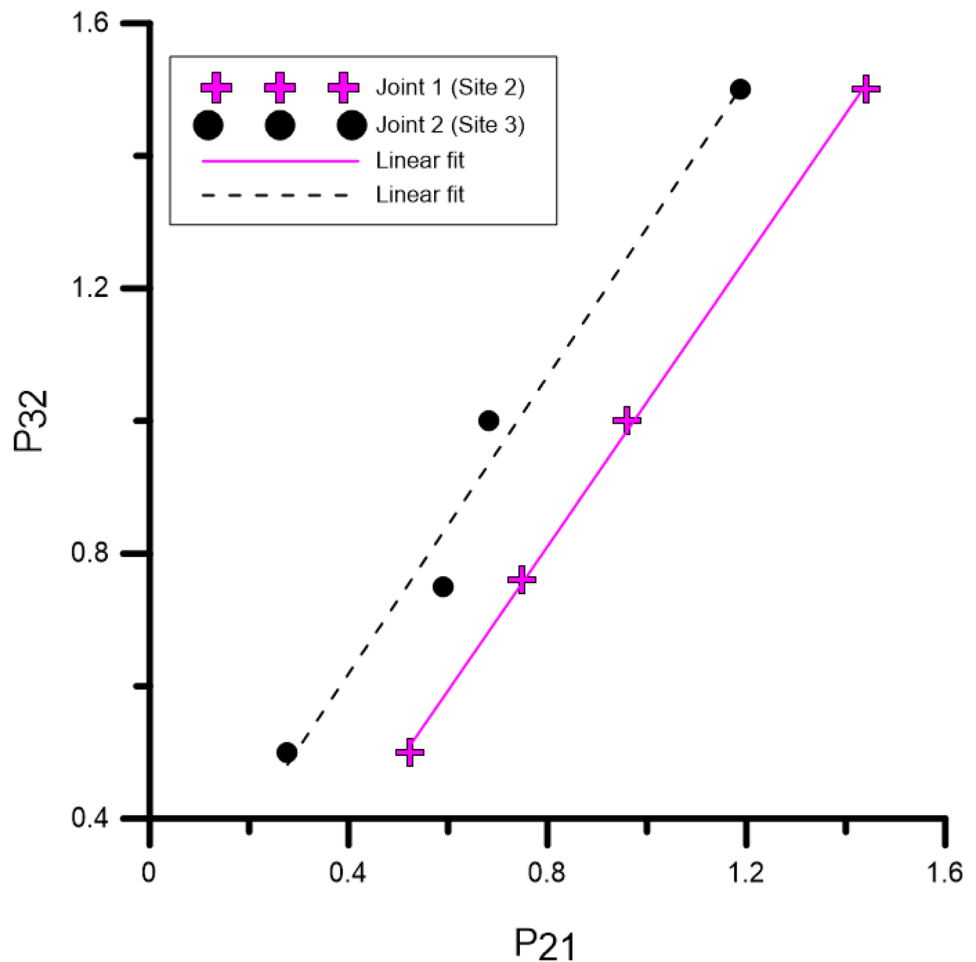
Discrete fracture network development

Rock mass has a wide discrepancy in properties due to variation in fractures network and their mechanical properties. DFN integrated rock mass will better represent the rock mass because it develops a stochastic fracture network based on probabilistic parameters. The much-required fracture trace length data used in fitting distribution curves were collected using point clouds and georeferenced images. The discontinuity orientation data was collected in the field and was also extracted from the developed 3D point cloud of the rock mass.

Fracture length and orientation distribution

DFN uses the discontinuity trace length and orientation distribution for fracture network generation. As discussed before, the discontinuity trace was following log-normal distribution at site 1. Further, at sites 2 and 3, power-law distributions were found to be the best fit. The fisher distribution was used as a statistical distribution of fracture orientation and found using dips software (Rocscience 2014). The data associated with DFN generation is listed in Table 5.

Fig. 12 Relation between P_{21} and P_{32} fracture intensities for joint 1 and 2 at sites 2 and 3



Volumetric fracture intensity (P_{32})

Volumetric fracture intensity (P_{32}) is defined as the ratio of the area of the fractures per unit volume. It is the most widely used and robust fracture intensity parameter for DFN generation. It is difficult to measure it directly in the field with scan-line or window mapping. The extension of the joint within the slope is obscure unless found using excavation. Unlike P_{32} the lower order fracture intensities like P_{21} and P_{10} can be directly measured from the outcrop survey. Dershowitz and Herda (1992) found that the higher-order fracture intensities can be calculated from the lower-order fracture intensities for the fixed orientation and orientation distribution of fractures. The author proposed the relation between P_{32} and P_{21} and P_{32} and P_{10} , as mentioned below.

$$P_{32} = P_{10} * C_{13} \qquad P_{32} = P_{21} * C_{32} \qquad (3)$$

where C_{32} and C_{21} are proportionality constants. Their values depend upon the orientation and size distributions of the fracture and also on outcrop orientation. Multiple simulations were repeated for varying P_{32} values and simultaneously

P_{21} and P_{10} values are measured on fixed planes to find a relation between them (Rogers et al. 2014). The relation between P_{21} and P_{32} for one of the joint set at sites 2 and 3 is shown in Fig. 12.

DFN validation

After generated fracture networks prior to geomechanical analysis, it is mandatory to validate the developed fracture system. The selective parameters like trace length distribution and orientation are compared for outcrop mapped fractures and generated DFNs. It can be seen in Fig. 13 that the traces of generated DFNs follow log-normal and power-law distribution at sites 1, 2, and 3, and thus validates the mapped trace data of the field (Figs. 7 and 8). The fracture orientation data for the fractures generated using DFNs is plotted over stereonet for validation (Fig. 14). The field-mapped joint traces and the corresponding DFN generated joint traces for two joint sets at site 2 are shown in Fig. 15. Hence, the results confirm the validation of the generated DFN for its applicability. Similarly, the DFNs were validated for the other two sites.

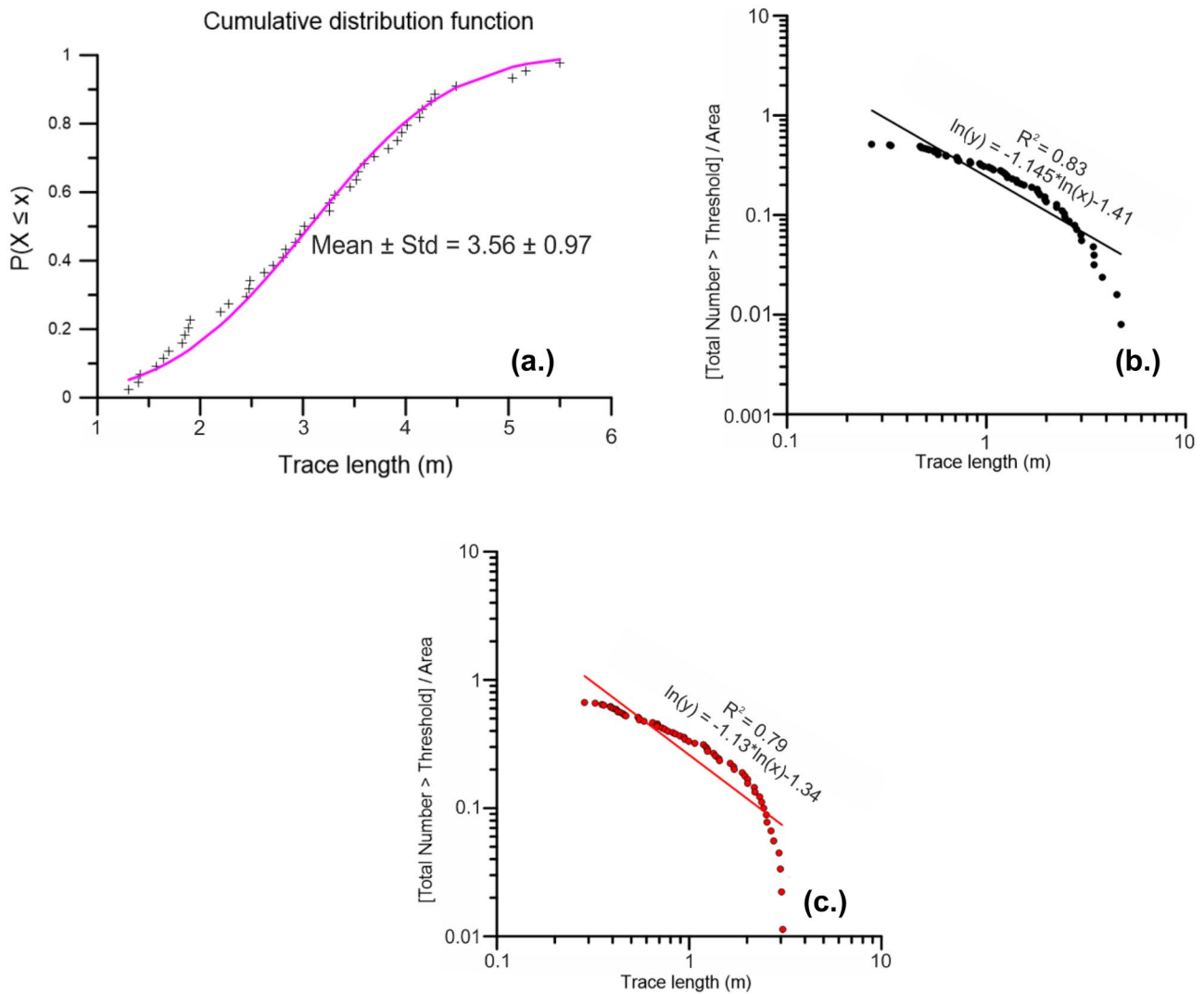


Fig. 13 Trace length distribution curves of the fractures generated using DFN to validate with field mapped fractures: **a** Joint 1 at site 1; **b** Joint 1 at site 2; **c** Joint 1 at site 3

Results and discussion

To analyse the control of structural damage on rock mass and slope movement, three-dimensional models were developed in 3DEC. The same slope topography was used for all three sites to compare the impact of rock mass conditions on the block kinematic.

Deterministic approach

The blocks were deemed to be rigid to simulate the influence of discontinuities on block displacement. The joints with fixed orientation and persistence parameters have been used to develop the deterministic fracture network for each

site. The model for site 1 shows block failure along the basal (floor) discontinuity (J1) and the other two discontinuity sets J2 and J3 had provided the lateral release surfaces (Fig. 16a). Whereas at sites 2 and 3, the slope was stable, and the block movement was nearly zero. The low persistence value for joints at sites 2 and 3 results in larger blocks that were stable under the current state of forces. Figure 16 illustrates the total displacement magnitude in the slopes with three different rock mass conditions.

For insight into the slope movement in different parts of the slope, six control points in most vulnerable area were selected to calculate horizontal velocity and horizontal displacement (Fig. 17). 3DEC is an explicit code; the solution to a problem requires several computational cycles. During each computational cycle, the information associated with

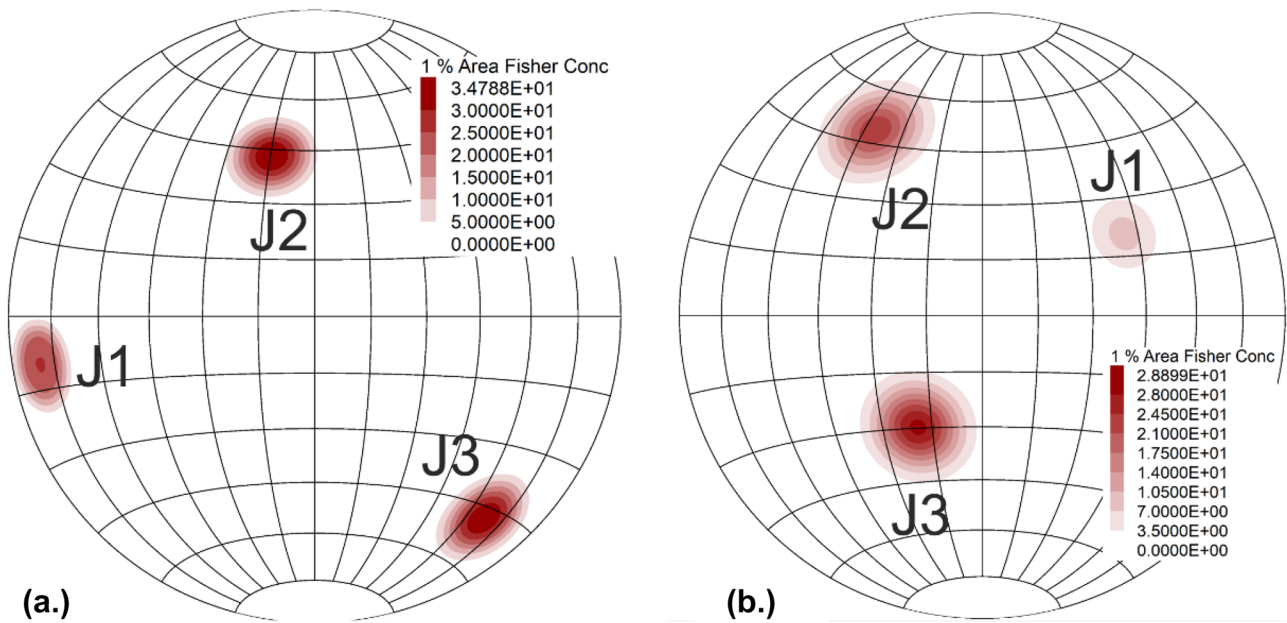


Fig. 14 Fractures generated using DFN plotted over stereonets: **a** site 1; **b** site 2

the phenomenon under investigation is propagated across the blocks in the model, so specific numbers of cycles are required to achieve an equilibrium state (Itasca Consulting Group Inc 2017b). For the six control points at site 1, the velocity was non-zero, and the displacement was still increasing with each computation cycle. Whereas at sites 2 and 3, the velocity dropped to zero, and displacement becomes consistent after a few initial computation cycles (Figs. 18, 19 and 20). When velocity approaches zero and displacement stays constant, it indicates the equilibrium condition (Itasca Consulting Group Inc 2017b). Hence, the slope at site 1 is unstable, and all parts of the slope at sites 2 and 3 represent steady conditions.

For greater insight into failure at site 1, the inverse velocity v/s cycles were plotted (Fig. 21). This “inverse velocity” method is widely accepted in monitoring displacement to predict the time of failure (Havaej et al. 2015) and the slope movement is predicted to be regressive or progressive (Zavodni and Broadbent 1980; Dick et al. 2013; Mercer 2006). A progressive movement shows accelerating displacements directing to slope instability, while a regressive movement is a periodic deceleration of the displacement leading to a stable slope. The on-set of failure point is identified where the movement changes from regressive to a progressive one. Figure 21 shows the inverse velocity and displacement v/s cycle plot for site 1. The on-set of failure of blocks starts

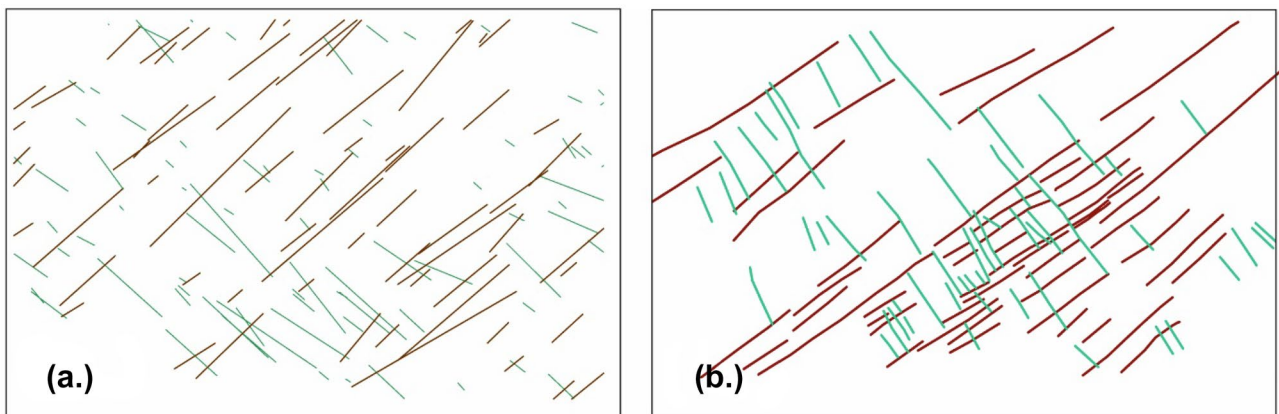


Fig. 15 Joint traces for two different joint sets at site 2: **a** traces of joints generated using DFN; **b** field mapped joint traces

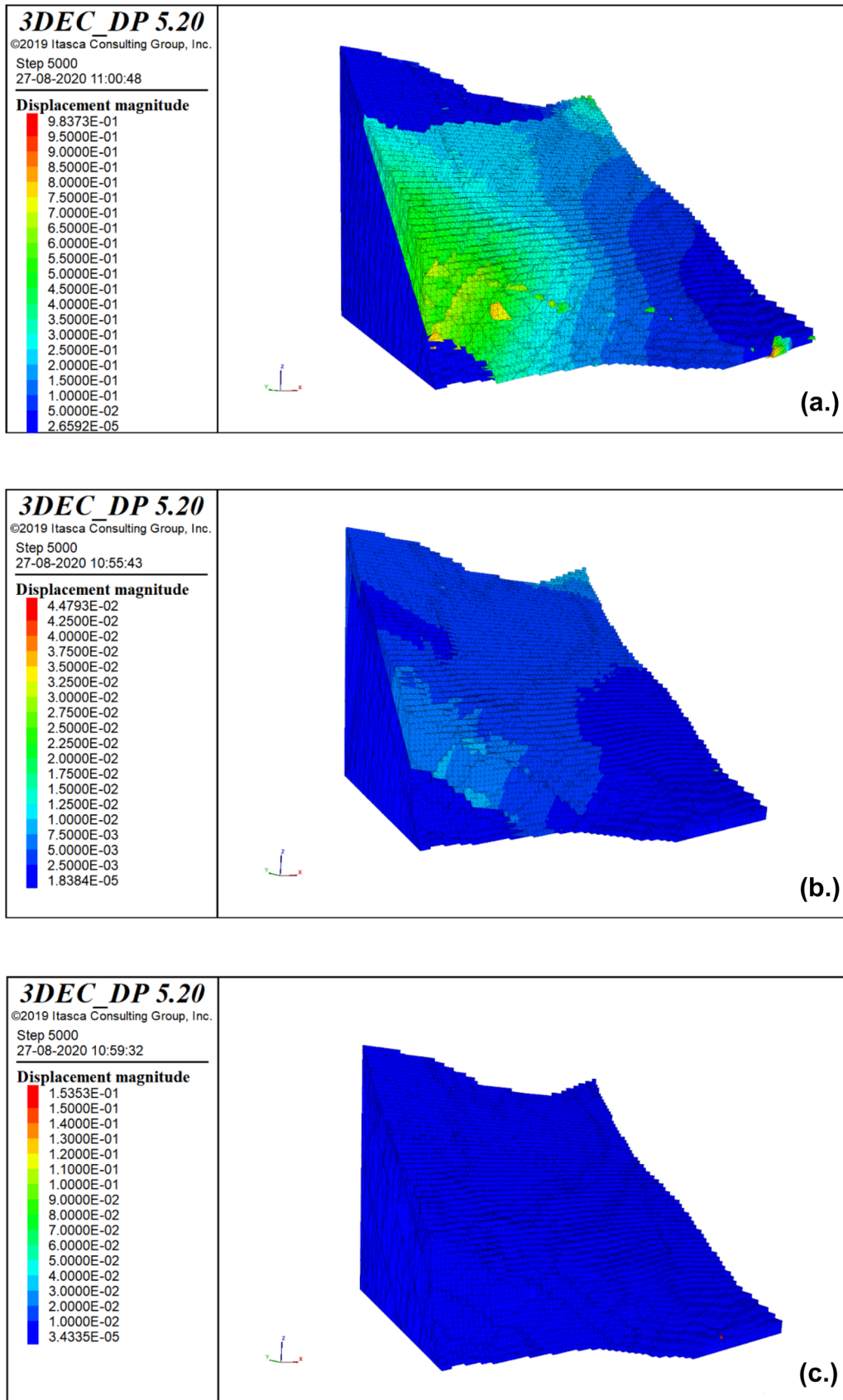


Fig. 16 Total displacement magnitude contours in the slope for different rock mass conditions: a site 1; b site 2; c site 3

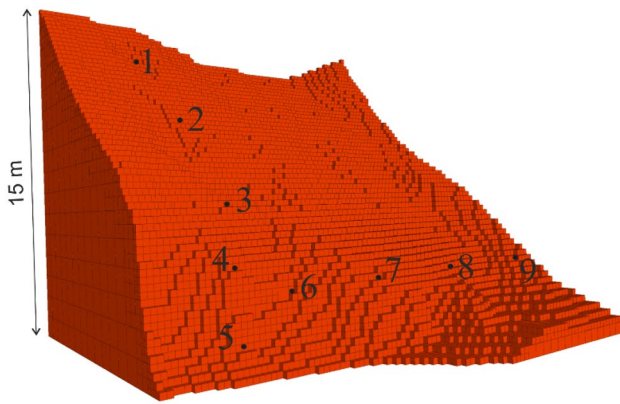


Fig. 17 3DEC geometry model of the slope marked with control points used to investigate the movement in different parts of the slope

around 800-time steps (cycles) at both points 4 and 7. The failure occurs when there is a sharp increase in displacement and inverse velocity starts approaching zero. The upward horizontal displacement trend and downward inverse velocity trend were interrupted around 6700 and 8300-time steps (cycles) at point 4 (Fig. 21a). This is the result of the stick–slip movement inhibiting continuous displacement due to comparative block confinement caused by dilation in the failing blocks (Havaej et al. 2015). The displacement smoothly increases at point 7 due to fewer failed blocks causing less dilation.

At the initial state of slope model construction, the model is not in equilibrium under the current state of forces. 3DEC calculates the total unbalanced force over all the blocks and tries to balance through each computation cycle. A model

is in exact equilibrium if the net nodal force vector at each block centroid approaches zero (Itasca Consulting Group Inc 2017b). The maximum unbalanced force can approach zero but will never have precisely zero value for numerical analysis. The model is considered to be in equilibrium only when the final maximum unbalanced forces are small compared to the initial representative forces (i.e., the ratio should be less than 0.001 or 0.1%) (Itasca Consulting Group Inc 2017b). The total unbalanced force was bobbling around a constant value at site 1 (Fig. 22a). If the unbalanced force approaches a constant nonzero value, this probably indicates that joint slip or block failure occurs within the model (Itasca Consulting Group Inc 2017b). Further, at sites 2 and 3 there was a humongous drop in the initial and final state of stresses pointing towards stable slopes (Fig. 22a). The results conclude that the slope at site 1 is not static; still, block movement is taking place, and that have also been found using displacement and velocity plots.

Stochastic approach

Based on the statistical parameters of discontinuities for all three sites, different DFNs were developed. As the developed DFN satisfied the required threshold and statistical parameters each time the DFN was generated, the fracture network realizations would be slightly different. So, three different realizations were done for each site and imported into 3DEC for slope modeling. Figure 23 shows the displacement contours and block movement at all three sites. It is vividly clear that site 1 was found to be unstable on the lower-left portion, similar to the deterministic model (Figs. 23a and 16a), further at site 2 and 3, no block

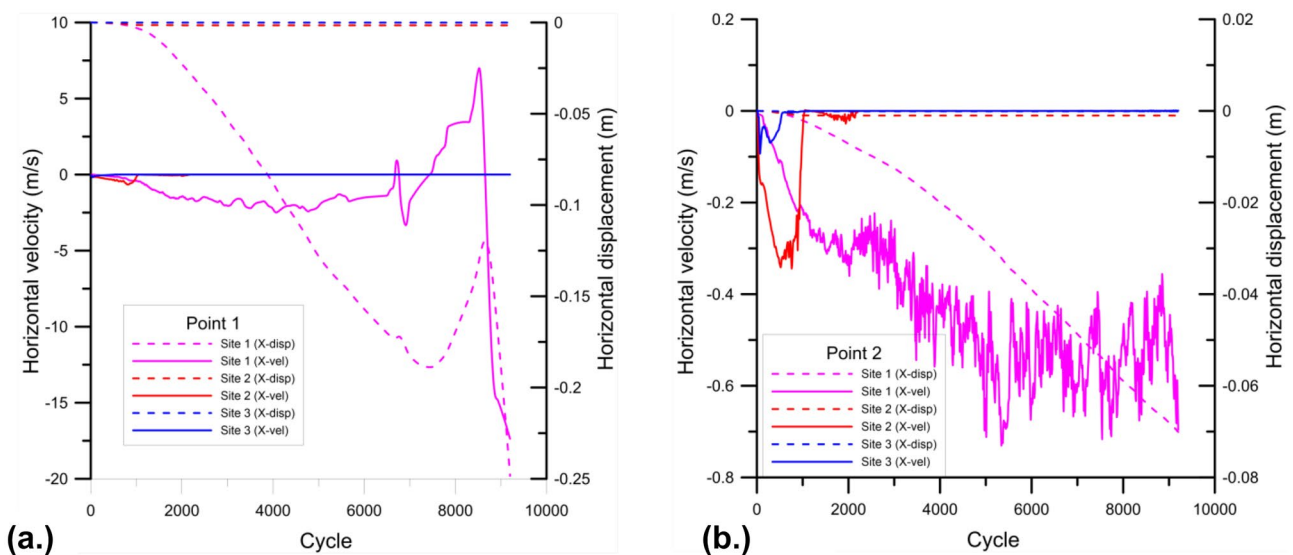


Fig. 18 Horizontal displacement and velocity v/s cycles plots for all the sites: **a** Point 1; **b** Point 2

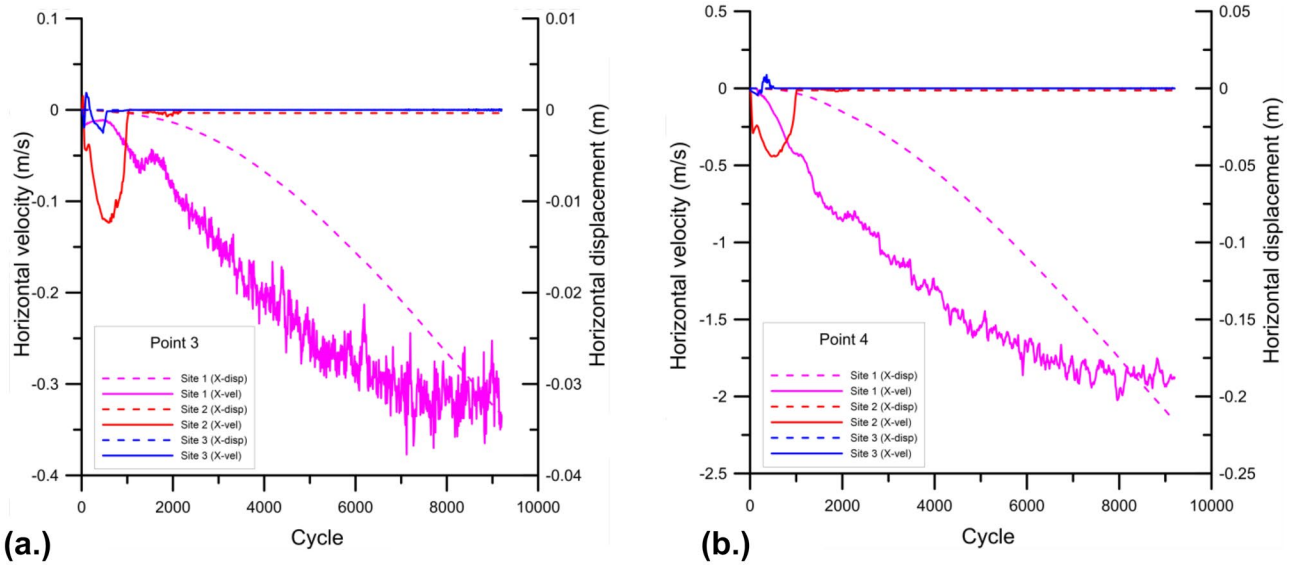


Fig. 19 Horizontal displacement and velocity v/s cycles plots for all the sites: **a** Point 3; **b** Point 4

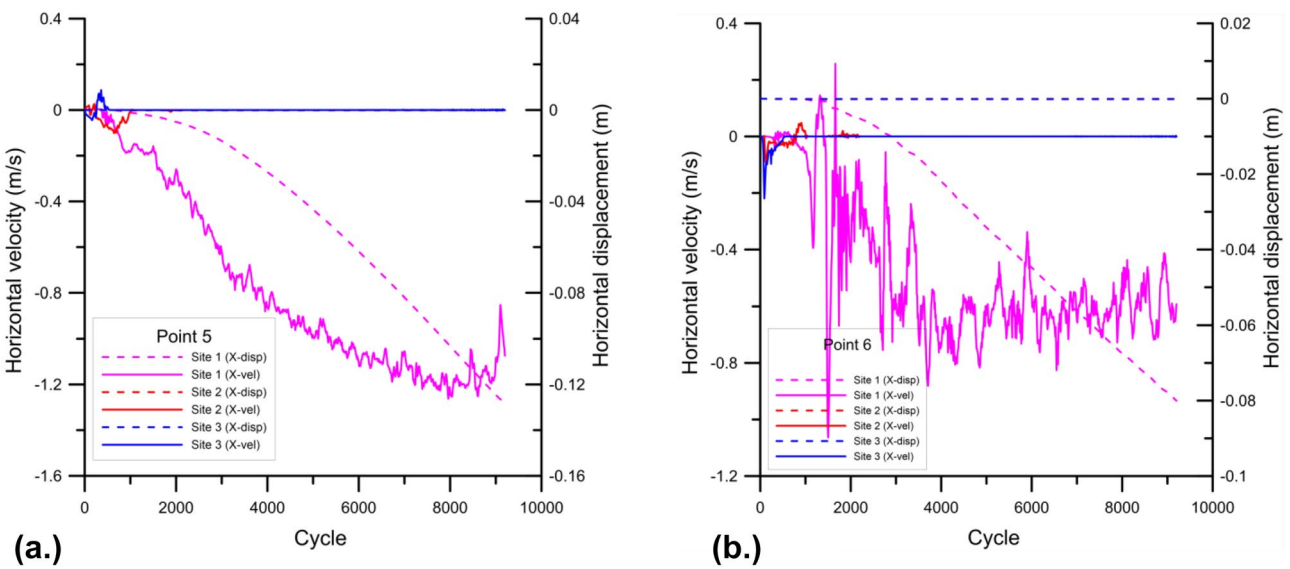


Fig. 20 Horizontal displacement and velocity v/s cycles plots for all the sites: **a** Point 5; **b** Point 6

Table 6 Maximum vertical displacement (m) at different control points marked over the slope

	Control point 1	Control point 2	Control point 3	Control point 4	Control point 5	Control point 6
Site 1 (Disp.)	0.014 m	0.031 m	0.0 m	0.004 m	0.0 m	0.004 m
Site 2 (Disp.)	0.0 m	0.0 m	0.0 m	0.0 m	0.0 m	0.0 m
Site 3 (Disp.)	0.0 m	0.0 m	0.0 m	0.0 m	0.0 m	0.0 m

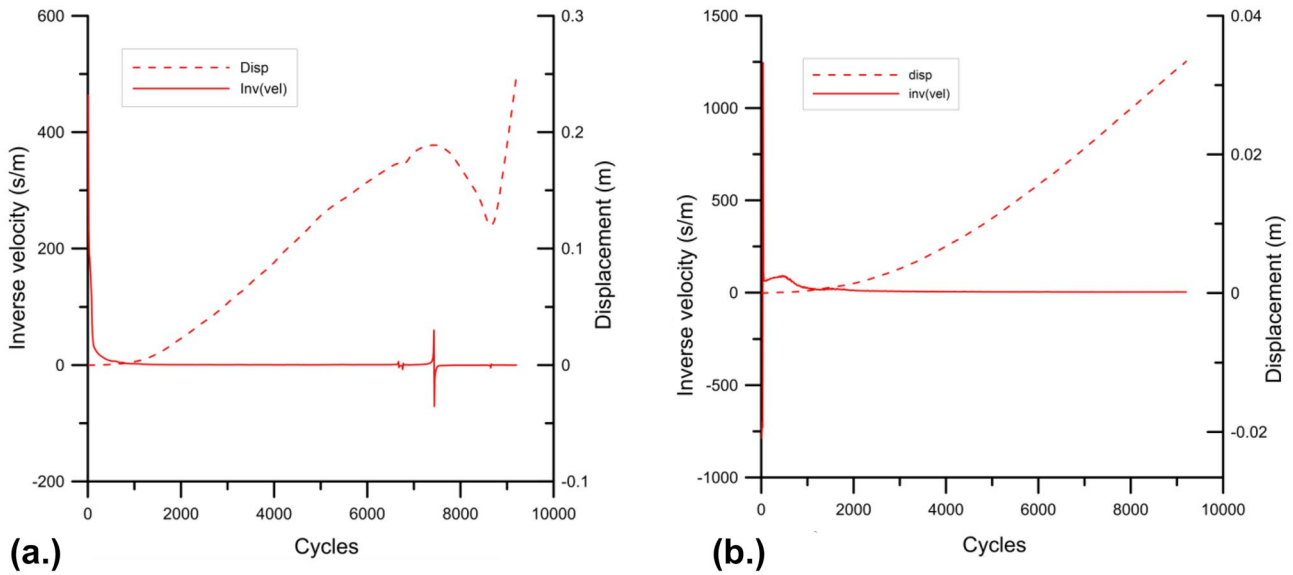


Fig. 21 Inverse velocity and displacement v/s cycles plot for site 4: **a** Point 1; **b** Point 7

movement was recorded in the slope (Fig. 23). The total displacement contours were widespread in the deterministic models, whereas in the stochastic model, the displacement is restricted to particular region. This is the limitation of deterministic models as joints are consistent throughout the slope; on the flip side, in stochastic models, there is variation in joint position and orientation depending upon statistical parameters. So, the failed blocks are restricted to a particular extent instead of slip along whole joint throughout the slope.

The maximum vertical displacement was recorded at points 1 and 2 at site 1 (Table 6). The displacement in blocks at points 4 and 6 initiated the movement in the upper portion of the slope, which was recorded at points 1 and 2 in form of vertical displacement. Further, at sites 2 and 3, zero displacement was recorded at all the point. Overall the total displacement including vertical and horizontal components was high near points 4, 5 and 6 (Fig. 23). The total unbalanced force was consistent at site 1, which points towards the unstable state of the blocks

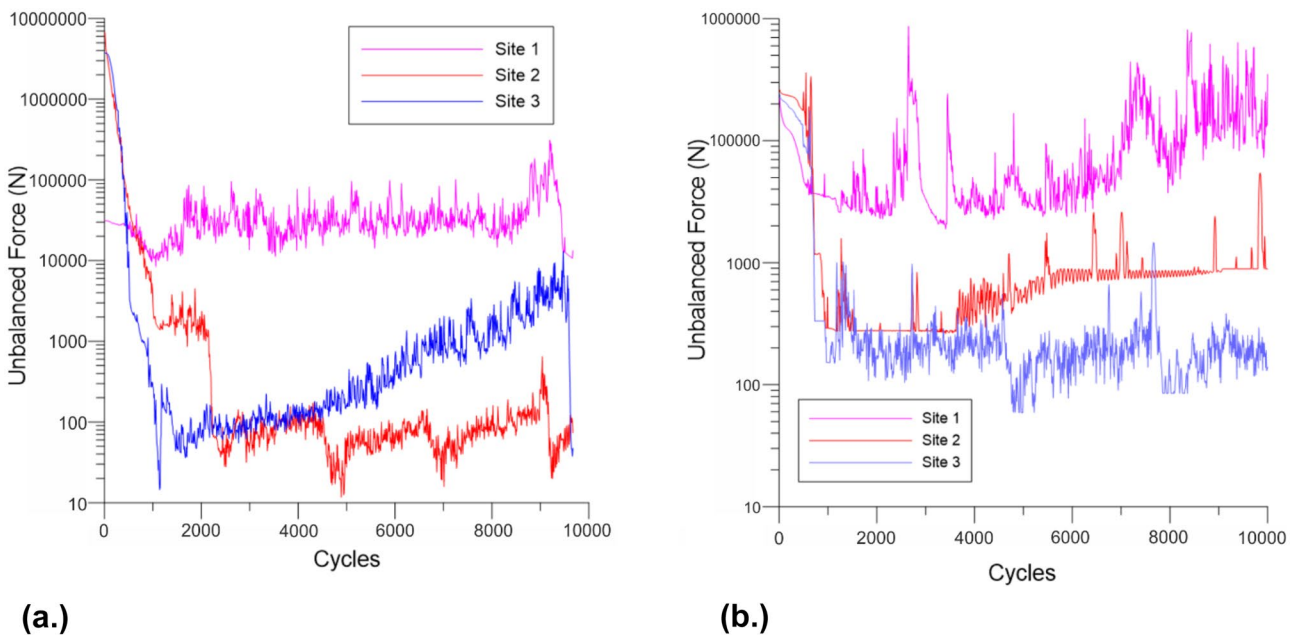


Fig. 22 Unbalanced force vs cycles plot for sites 1, 2 and 3: **a** deterministic approach; **b** stochastic approach

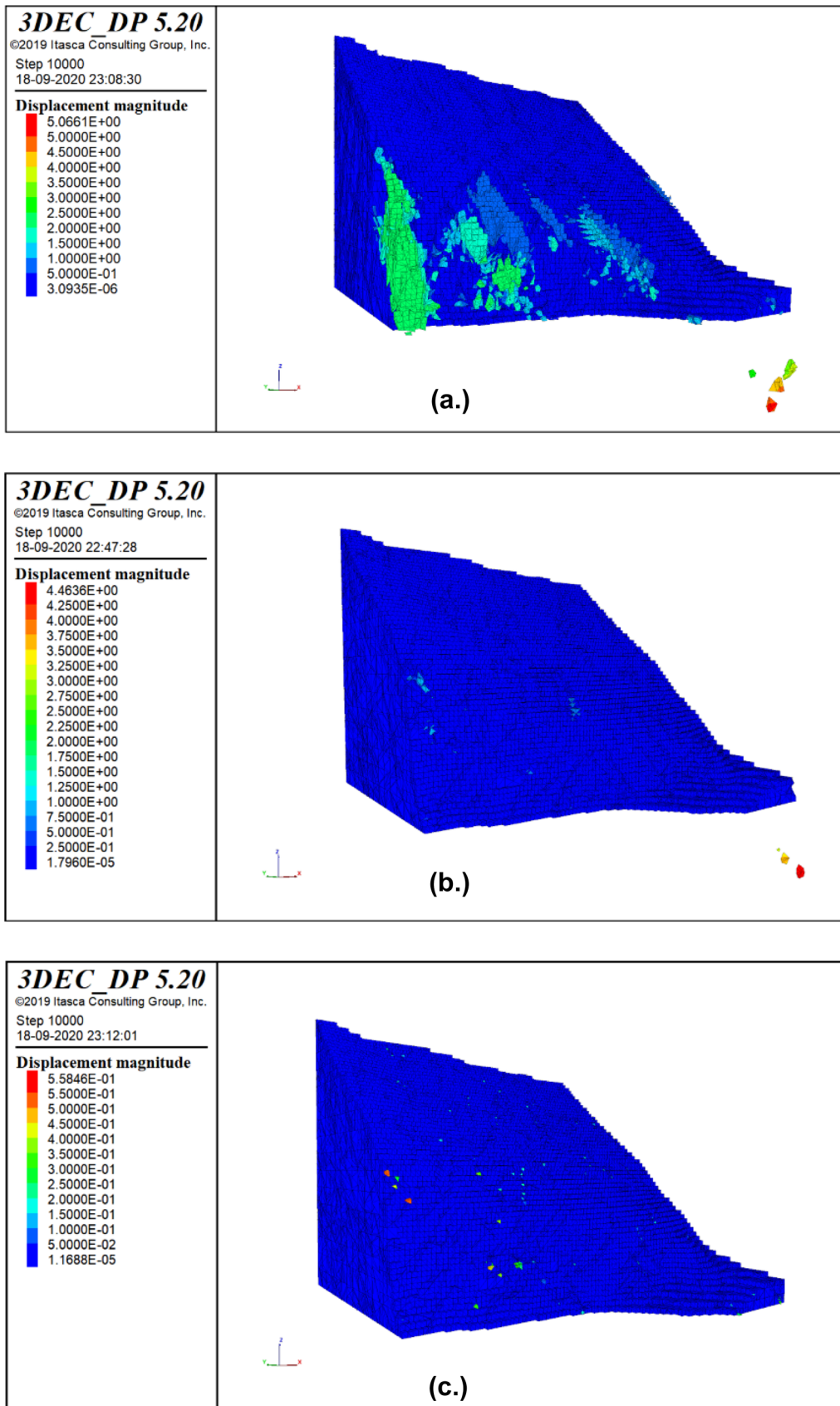


Fig. 23 Total displacement contours in different rock mass conditions: a site 1; b site 2; c site 3

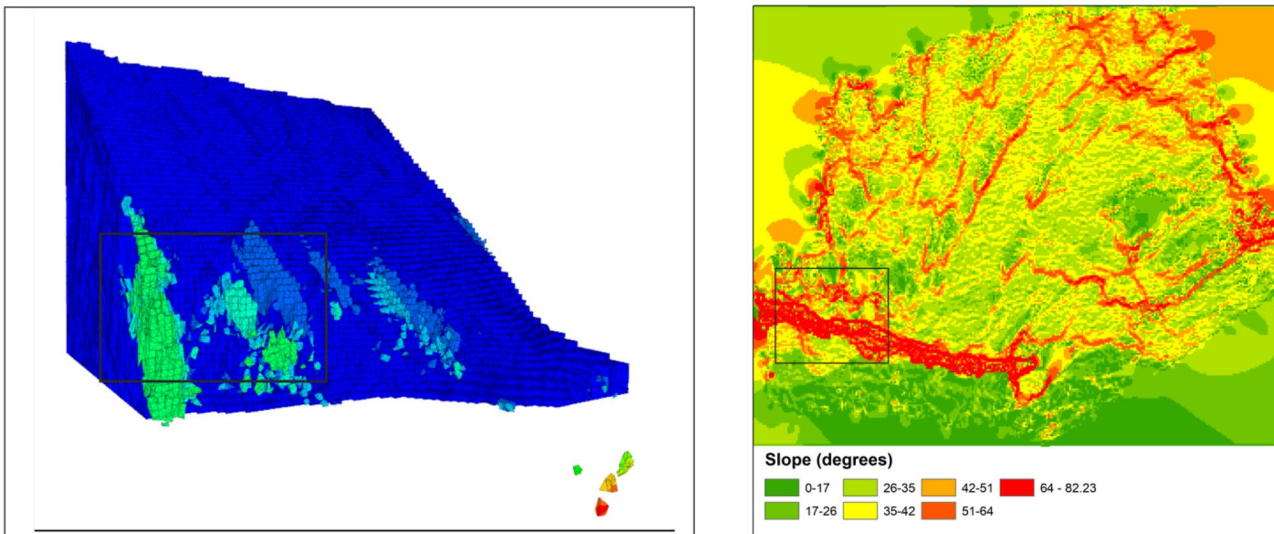


Fig. 24 Showing 3DEC block displacement model for site 1 and DEM created using point cloud

in the slope; but at sites 2 and 3, there was a double order drop in the initial and final state of stresses marking the stable conditions in the slopes (Fig. 22b). The results conclude that the slope at site 1 is not static and block movement is taking place similar to the results using the deterministic approach.

Control of slope topography

The slope topography impact is conspicuous for block stability. It can be delineated from the DEM created using point cloud and both deterministic and stochastic slope models that most of the unstable blocks were in high slope angle area (Fig. 24). The block movement can only be found in the place where the slope angle was greater than 60° . Due to the topography impact, single slope topography was used to analyze slope stability to compare the influence of rock mass at all the sites.

Conclusions

The study presents the investigation of rock mass within and away from the damage zone (hinge) of the Garhwal Syncline. The core region experiences the maximum damage due to profound strain accumulation during folding. Higher stresses during folding at site 1 lead to propagation of existing or new fractures and intersected the rock mass into comparatively smaller sized blocks. Moving away along the right limb follows the increase in joint spacing and block size in the rock mass. The joint trace length and the volumetric fracture intensity was estimated at three different sites. High frequency of mean-sized fracture traces was found at site 1 in the hinge zone and results in log-normal distribution.

Whereas, at the sites away from damage zone the lower volumetric fracture intensity was recorded and the joint traces were following power-law fit. The block volume distribution curve was plotted for each site from the blocks formed by the intersection of DFN. Site 1 shows smaller volume blocks complying with the fracture intensity and field observation as discussed earlier.

To model the influence of rock mass characteristics, the slope stability analysis was conducted for all the three sites in 3DEC. Deterministic and stochastic (DFN) approach was followed for fracture/joint construction in 3DEC model. Multiple parameters like horizontal velocity, horizontal displacement, inverse velocity, and unbalanced force were used to have insight into the dynamics of the slope movement. The results conclude that the anomalous high fracture intensity due to intense fracturing in the fold damage zone reduces the strength of the rock mass and increases the kinematic freedom causing frequent block movements. Whereas, at sites 2 and 3, due to low fracture intensity, the increase in block size could provide kinematic stability to the block movement. The study focuses to highlight the importance of geological structures in engineering geological practices. We recommend engineering practitioners to investigate the rock mass separately in the vicinity of structurally damaged zones due to wide variation in the rock mass characteristics.

Acknowledgements The authors express their sincere acknowledgements to the Department of Earth Sciences, IIT Roorkee, and IIT Bombay for providing the necessary laboratory and computer facilities. We would like to thank IIT Roorkee and American Geophysical Union (AGU) for providing financial support to present this work at AGU, Fall Meeting 2019, San Francisco, USA. JS extends acknowledgment

to the Council of Scientific and Industrial Research (CSIR), Govt. of India for providing SPM fellowship to conduct the PhD research work.

Declarations

Conflict of interest The authors declare no competing interests.

References

- Barton N, Bandis S (1990) Review of predictive capabilities of JRC/JCS model in engineering practice. *Int. Proc. Symp. on Rock Joints*, Loan, Norway, pp 603–610.
- Barton N, Choubey V (1977) The shear strength of rock joints in theory and practice. *Rock Mech* 10:1–54. <https://doi.org/10.1007/BF01261801>
- Bonilla-Sierra V, Scholtès L, Donzé F, Elmouttie M (2015) DEM analysis of rock bridges and the contribution to rock slope stability in the case of translational sliding failures. *Int J Rock Mech Min Sci* 80:67–78
- Brideau MA (2005) The Influence of tectonic structures on rock mass quality and implications for rock slope stability. MSc Thesis. Simon Fraser University, Canada.
- Brideau MA, Yan M, Stead D (2009) The role of tectonic damage and brittle rock fracture in the development of large rock slope failures. *Geomorphology* 103:30–49
- Brideau M, Pedrazzini A, Stead D (2011) Three-dimensional slope stability analysis of South Peak, Crowsnest Pass, Alberta, Canada. *Landslides* 8:139–158
- Brideau MA, Stead D (2012) Evaluating kinematic controls on planar translational slope failure mechanisms using three-dimensional distinct element modeling. *Geotech Geol Eng* 30:991–1011
- Brideau MA, McDougall S, Stead D, Evans SG, Couture R, Turner K (2012) Three-dimensional distinct element modeling and dynamic analysis of a landslide in gneissic rock, British Columbia, Canada. *Bull Eng Geol Environ* 71:467–486
- Budetta P, Nappi M (2011) Heterogeneous rock mass classification by means of the geological strength index: the San Mauro formation (Cilento, Italy). *Bull Eng Geol Environ* 70:585–593
- Chester FM, Logan JM (1986) Composite planar fabric of gouge from the Punchbowl Fault, California. *J Struct Geol* 9:621–634
- Coggan JS, Pine RJ (1996) Application of distinct-element modeling to assess slope stability at Delabole slate quarry, Cornwall, England. *Trans Inst Min Metall* 105:22–30
- Costa M, Coggan JS, Eyre JM (1999) Numerical modeling of slope behaviour of Delabole slate quarry (Cornwall, UK). *Int J Surf Min Reclam Environ* 13(1):11–18
- GPL Software (2018) Cloud Compare V.2.9. <http://www.cloudcompare.org>
- Dershowitz WS, Herda HH (1992) Interpretation of fracture spacing and intensity. In: *Proc. 33rd U.S. Rock Mech. Symp.*, Santa Fe, NM
- Dershowitz WS, Lee G, Geier J, LaPointe P (2014) *FracMan: interactive discrete feature data analysis, geometric modeling and exploration simulation*. Golder Associates Inc.
- Donati D, Stead D, Brideau MA, Ghirotti M (2017) A model-oriented, remote sensing approach for the derivation of numerical modeling input data: Insights from the Hope Slide, Canada, *Proc ISRM Regional Conference.*, Afirirocks, Cape Town, S.A, pp 15
- Dick GJ, Eberhardt E, Stead D, Rose ND (2013) Early detection of impending slope failure in open pit mines using spatial and temporal analysis of real aperture radar measurements. *Slope Stability 2013*, Australian Centre for Geomechanics, pp 949–962
- Elmo D (2006) Evaluation of a hybrid FEM/DEM approach for determination of rock mass strength using a combination of discontinuity mapping and fracture mechanics modelling, with particular emphasis on modelling of jointed pillars. Ph.D. Thesis. Camborne School of Mines, University of Exeter, UK
- Elmo D, Clayton C, Rogers S, Beddoes R, Greer S (2011) Numerical simulations of potential rock bridge failure within a naturally fractured rock mass. In: *Proc. Int. Symp. on Rock Slope Stability in Open Pit Mining and Civil Engineering*. Vancouver, Canada
- Elmo D, Stead D (2010) An integrated numerical modelling–discrete fracture network approach applied to the characterisation of rock mass strength of naturally fractured pillars. *Rock Mech Rock Eng* 43:3–19
- Elmo D, Donati D, Stead D (2018) Challenges in the characterisation of intact rock bridges in rock slopes. *Eng Geol* 245:81–96
- Fossen H (2010) *Structural Geology*. University of Bergen, Cambridge University Press, New York
- Francioni M, Stead D, Sciarra N, Calamita F (2018) A new approach for defining slope mass rating in heterogeneous sedimentary rocks using a combined remote sensing–GIS approach, *Bull Eng Geol Environ* pp 1–22
- Francioni M, Simone M, Stead D, Sciarra N, Mataloni G, Calamita FA (2019) New fast and low-cost photogrammetry method for the engineering characterization of rock slopes. *Remote Sens* 11:1267
- Havaej M (2015) Characterisation of high rock slopes using an integrated numerical modeling–remote sensing approach. Ph.D. Thesis. Simon Fraser University, Canada
- Havaej M, Coggan J, Stead D, Elmo D (2015) A combined remote sensing–numerical modeling approach to the stability analysis of Delabole Slate Quarry, Cornwall, UK. *Rock Mech Rock Eng* 178:1–19
- Itasca Consulting Group Inc (2017a) 3DEC 5.2, Distinct element modeling of jointed and blocky material in 3D. <https://www.itascacg.com/software/3dec>
- Itasca Consulting Group Inc (2017b) 3DEC 5.2, User's guide
- Johri M (2012) Fault damage zones – observations, dynamic modeling, and implications on fluid flow. Ph.D. Thesis. Stanford University, USA
- Mandl G (2005) *Rock joints—the mechanical genesis*, 2005th edn. Springer, Berlin
- Mercer KG (2006) Investigation into the time dependent deformation behaviour and failure mechanisms of supported rock slopes based on the interpretation of observed deformation behaviour. Ph.D. Thesis. University of the Witwatersrand
- Pedrazzini A, Jaboyedoff M, Froese CR, Langenberg CW, Moreno F (2011) Structural analysis of turtle mountain: origin and influence of fractures in the development of rock slope failures. *Geological Society, London, Special Publications* 351:63–183
- Pradhan SP, Siddique T (2020) Stability assessment of landslide-prone road cut rock slopes in Himalayan terrain: a finite element method based approach. *J Rock Mech Geotech Eng* 12:59–73
- Pradhan SP, Vishal V, Singh TN (2018) Finite element modelling of landslide prone slopes around Rudraprayag and Agastyamuni in Uttarakhand Himalayan terrain. *Nat Hazards* 94:181–200
- Pradhan SP, Panda SD, Roul AR, Thakur M (2019) Insights into the recent Kotropi landslide of August 2017, India: a geological investigation and slope stability analysis. *Landslides* 16:1529–1537. <https://doi.org/10.1007/s10346-019-01186-8>
- Price NJ, Cosgrove JW (1990) *Analysis of geological structures*. Cambridge university press, pp 502
- Priet SD, Hundson JA (1976) Discontinuity spacing in rock. *Int J Rock Mech Min Sci Geomech* 13:135–148
- Pine RJ, Coggan JS, Flynn ZN, Elmo D (2006) The development of a new numerical modelling approach for naturally fractured rock masses. *Rock Mech Rock Eng* 39(5):395–419

- Rocscience (2014) c Dips 6.0 graphical and statistical analysis of orientation data. Rocscience Inc., Toronto, Canada
- Savage HM, Brodsky EE (2011) Collateral damage: evolution with a displacement of fracture distribution and secondary fault strands in fault damage zones. *J Geophys Res-Sol Ea* 116(3)
- Shaunik D, Singh M (2019) Strength behaviour of a model rock intersected by non-persistent joint. *J Rock Mech Geotech Eng* 11:1243–1255
- Shaunik D, Singh M (2020) Bearing capacity of foundations on rock slopes intersected by non-persistent discontinuity. *Int J Min Sci* 30(5):669–674
- Rogers S, Elmo D, Webb G, Catalan A (2014) Volumetric fracture intensity measurement for improved rock mass characterisation and fragmentation assessment in block caving operations. *Rock Mech Rock Eng* 48:633–649
- Shankar R (1971) Stratigraphy and sedimentation of Tal Formation, Mussoorie syncline, U P. *J Paleontol Soc India* 16:1–15
- Shanker R, Kumar G, Mathur VK, Joshi A (1993) Stratigraphy of the Blaini, Infrakrol, Krol and Tal succession, Krol belt, Lesser Himalaya. *Indian J Petrol Geol* 2:9–136
- Shipton ZK, Cowie PA (2003) A conceptual model for the origin of fault damage zone structures in high-porosity sandstone. *J Struct Geol* 25:333–344
- Singh J, Thakur M (2019) Landslide stability assessment along Panchkula-Morni road, Nahan salient, NW Himalaya. *India J Earth Syst Sci* 128:148
- Singh J, Pradhan SP, Panda SD, Singh M (2019) Abstract: slope stability assessment of Himalayan road cut slope using advanced remote sensing techniques and numerical simulation. American Geophysical Union (AGU) Fall Meeting 2019, abstract #NH51B-0778, San Francisco, USA. Bibcode: [2019AGUFMNH51B0778S](#)
- Singh TN, Pradhan SP, Vishal V (2013) Stability of slope in a fire prone opencast mine in Jharia coalfield, India. *Arab J Geosci* 6:419–427
- Smith L, Forster CB, Evans JP (1990) Interaction of fault zones, fluid flow, and heat transfer at the basin scale. Hydrogeology of permeability environments. (S. P. Newman and I. Neretnieks, eds.), International Association of Hydrogeological Sciences selected papers in Hydrogeology 2:41–67
- Srivastava RM (2002) Probabilistic discrete fracture network models for the whiteshell research area, Ontario. FSS Canada Consultants Inc, Canada
- Stead D, Wolter A (2015) A critical review of rock slope failure mechanisms: the importance of structural geology. *J Struct Geol* 74:1–23
- Sturzenegger M, Stead D (2012) The Palliser Rockslide, Canadian Rocky Mountains: characterization and modeling of a stepped failure surface. *Geomorphology* 138:145–161
- Vazaios I, Vlachopoulos N, Diederichs MS (2017) Integration of Lidar-based structural input and Discrete Fracture Network generation for underground applications. *Geotech Geol Eng* 35:2227–2251
- Vazaios I, Farahmand K, Vlachopoulos N, Diederichs MS (2018) Effects of confinement on rock mass modulus: a synthetic rock mass modelling (SRM) study. *J Rock Mech Geotech Eng*, pp 436–456.
- Valdiya KS (1984) Evolution of the Himalaya. *Tectonophysics* 105(3):229–248
- Vanneschi C, Eyre M, Venn A (2019) Investigation and modeling of direct toppling using a three-dimensional distinct element approach with the incorporation of point cloud geometry. *Landslides* 16:1453–1465. <https://doi.org/10.1007/s10346-019-01192-w>
- Vishal V, Pradhan SP, Singh TN (2015) An investigation on stability of mine slopes using two dimensional numerical modeling. *J Rock Mech Tunnel Tech* 21(1):49–56
- Viviana BS, Scholtès L, Donzé FV, Elmoutie MK (2015) Rock slope stability analysis using photogrammetric data and DFN–DEM modelling. *Acta Geotech* 10(4) 497–511. <https://doi.org/10.1007/s11440-015-0374-z>
- Zavodni ZM, Broadbent CD (1980) Slope failure kinematics. *Bulletin Canadian Institute of Mining, Canadian Institute of Mining and Metallurgy* 73:69–74